ACOUSTIC DETECTION OF HIGH - ALTITUDE TURBULENCE

JOHN W. WESCOTT

ACOUSTICS AND SEISMICS LABORATORY
Institute of Science and Technology
THE UNIVERSITY OF MICHIGAN

March 1964

Contract DA-20-018 ORD-22840

3746-38-T

ACOUSTIC DETECTION OF HIGH-ALTITUDE TURBULENCE

JOHN W. WESCOTT

March 1964

Acoustics and Seismics Laboratory
Institute of Science and Technology
THE UNIVERSITY OF MICHIGAN
Ann Arbor, Michigan

NOTICES

Sponsorship. The work reported herein was conducted by the Institute of Science and Technology for the U. S. Army Electronics Research and Development Activity under Contract DA-20-018-ORD-22840. Contracts and grants to The University of Michigan for the support of sponsored research by the Institute of Science and Technology are administered through the Office of the Vice-President for Research.

Distribution. Initial distribution is indicated at the end of this document.

DDC Availability. Qualified requesters may obtain copies of this document from:

Defense Documentation Center
Cameron Station
Alexandria, Virginia

Final Disposition. After this document has served its purpose, it may be destroyed. Please do not return it to the Institute of Science and Technology.

CONTENTS

FIGURES

ACOUSTIC DETECTION OF HIGH-ALTITUDE TURBULENCE

ABSTRACT

Background noise at frequencies from 0.2 to 200 cps was monitored with free-floating, balloon-borne acoustic probes at altitudes of 55,000 to 73,000 feet. Spectrograms, signatures, cross-correlations, and probability-density curves were obtained from the data. The noise has a spectrum with 6 db/octave negative slope, is acoustic and Gaussian, and is time-steady for periods of several hours, although noise pressures from 0.03 to 1 dyne/cm^2 were measured on different days. These and other results indicate that the noise comes from lower altitudes and is produced by an array of statistically independent radiators, such as turbulent eddies.

A theory for the power spectrum of noise radiated by turbulence is cited, and the predicted spectrum is compared to the experimental results. Other possible sources of high-altitude acoustic noise are described. Descriptions and illustrations of the instruments used to acquire and process the experimental data are presented.

1 INTRODUCTION

This report describes an investigation into the nature and sources of acoustic background noise at high altitudes. The results relate to the problem of acoustic detection and location of target sound sources at long ranges. Early in the project it appeared that sound radiated by atmospheric turbulence might be a significant component of high-altitude acoustic noise [1]. Moreover, theories on noise radiated by turbulence seemed to support the first experimental results [2]. Additional data were therefore acquired and processed to determine pressure spectra, diurnal variations, propagation characteristics, and other physical properties of background noise that might be related to atmospheric turbulence.

Broadband acoustic noise at frequencies from 0.2 to 200 cps and acoustic signals within this noise were monitored with free-floating, balloon-borne microphones at altitudes up to 73,000 feet. Over 30 instrumented balloon flights were completed successfully. Among these were several double-probe flights in which one microphone was suspended several hundred feet below another. All data acquired by the acoustic probes were transmitted by radio link to a ground tracking station, where they were recorded on magnetic tape and later analyzed. Four types of data analysis were performed: (1) spectrum analysis, (2) signature analysis, (3) cross-correlation, and (4) statistical or probability-density analysis. The results combined to indicate that atmospheric turbulence is the principal source of ambient acoustic noise measured at high altitudes.

2
SUMMARY

Spectrum analyses of 25 samples of high-altitude data reveal 30-db diurnal variations in acoustic noise level (from 0.03 to 1 dyne/cm^2 in the 1-cps region), but a consistent shape to the spectrum. The measured spectrum has a negative slope of 6 db/octave compared to a theoretically predicted negative slope of 10.7 db/octave [2].

Signature analyses display a time-steady acoustic background level during balloon flights of three hours or less, but superimposed on this background are the time-varying spectra of passing aircraft and various unidentified, sporadic infrasonic disturbances. The Doppler curves of piston-engined aircraft show both a directly received signal and an equally strong reflected signal from the earth's surface.

Cross-correlated data from double probe flights show a 22%-correlation index for a bandwidth of 0.2 to 30 cps. This occurs when the time delay between data channels is such that the sound appears to come from a great number of statistically independent radiators randomly distributed over a large area beneath the detectors.

Probability-density curves plotted from oscillograms of high-altitude background noise show a Gaussian distribution of acoustic pressure fluctuations, again indicating sound received from a large number of statistically independent radiators. On the other hand, a probability-density curve plotted from an oscillogram of localized flow noise shows a non-Gaussian distribution of pressure fluctuations. This means that these two types of noise, acoustic and hydrodynamic, can be identified from data supplied by a single acoustic probe [2].

The evidence summarized above strongly suggests that the signals detected are samples of far-field acoustic noise from turbulence in the atmosphere. The four key factors are the 6 db/octave negative slope of the noise spectrum, its time-steady behavior, its acoustic rather than hydrodynamic nature, and its Gaussian pressure distribution. The diurnal variations in acoustic noise level probably relate to variations in turbulent activity within detection range of the probes, although the exact relationship remains to be determined. It is concluded that the sonic techniques described in this report offer an effective means for studying high-altitude atmospheric turbulence.

3
EXPERIMENTAL RESULTS

3.1. SPECTRUM ANALYSIS

Spectrum analyses were made from 25 samples of acoustic background noise obtained with calibrated, balloon-borne acoustic detectors at altitudes of 55,000 to 73,000 feet. The appendix

contains a complete set of these spectrograms together with a description of the data-processing method employed. The curves show acoustic pressure in a constant bandwidth of 1 cycle plotted against frequency, for a range from 0.63 to 100 cps.

Figure 1 shows four of these spectrum level curves, which were chosen to illustrate both the shape of the spectrum and the diurnal variation of noise level. The acoustic pressure spectrum has a consistent shape which falls off as the first power of frequency (6 db/octave) when measured on a constant bandwidth basis. The measured power spectrum, accordingly, falls off as the second power of frequency. This is within fair but not close agreement with a theoretical prediction for the power spectrum of noise radiated by turbulence, as discussed in Section 4.1. This theory predicts a power spectrum that falls off as the 7/2 power of frequency [3].

Figure 1 shows diurnal variations of rms acoustic pressure from 0.03 to 1 dyne/cm^2 in the frequency region just below 1 cps. This is a 30-db dynamic range and, assuming the noise was produced by atmospheric turbulence, indicates either large changes in nearby turbulent activity or large changes in distance between an acoustic probe and the turbulence detected. In any case, detection of strong, time-steady background noise having an acoustic spectrum as described above suggests strong, nearby turbulence as the noise source.

3.2. SIGNATURE ANALYSIS

Time-varying spectra or signatures of data were investigated with a real-time, heterodyning spectrum analyzer having an effective filter bandwidth of 1 cps, which was swept repeatedly through a frequency range from d-c to 150 cps. The instrument produced a complete spectrum analysis of consecutive data segments every two seconds and displayed the result as intensity-modulated line scans on Teledeltos paper. The record is thus a three-dimensional display of time, frequency, and amplitude. Time is read along the length of the record, frequency is read across the record, and acoustic pressure at any given time and frequency is proportional to the darkness of the record at that point.

Figure 2 is an analysis of a four-minute sample of data and shows the signature of a piston-engined aircraft as detected by a balloon-borne microphone. Piston-engined aircraft are particularly easy to identify because of the obvious Doppler shift which occurs in the apparent piston firing rate as the aircraft approaches, passes, and recedes. For Figure 2 the frequency range of the spectrometer was extended to 300 cps to display the second harmonic of the piston-firing rate. This type of sound is rich in harmonics.

The aircraft signature of Figure 2 has a double trace at the fundamental piston-firing rate. The trace showing the more rapid Doppler shift is from the signal which propagated directly from aircraft to detector. The other trace is for the same aircraft signal received by reflection

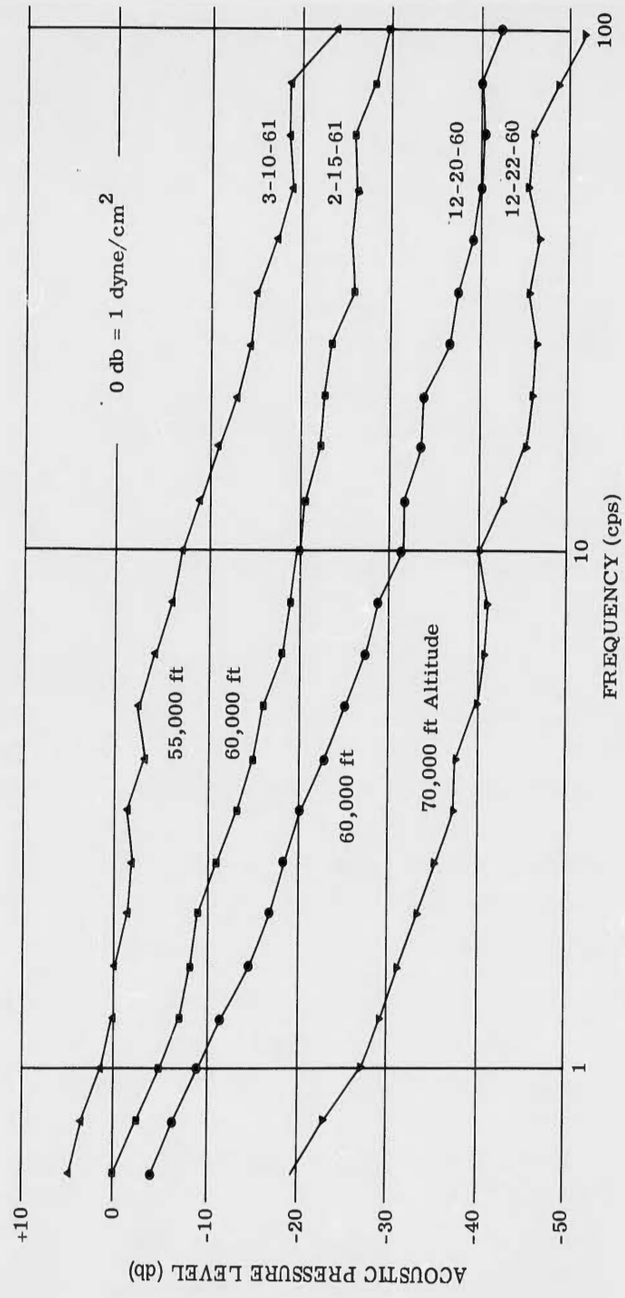

FIGURE 1. MEASURED ACOUSTIC PRESSURE SPECTRUM

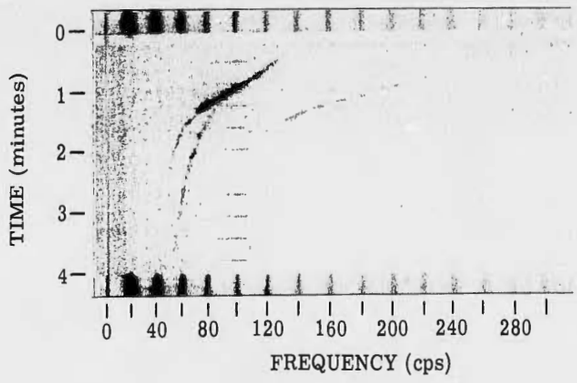

FIGURE 2. AIRCRAFT DOPPLER SIGNATURE

from the earth's surface. Note that for this data sample the reflected signal from the receding aircraft persists for a longer time than the direct signal. Sometimes, as will be seen in other data samples, the direct signal persists longer than the reflected one. Whether the direct or reflected signal persists for the longer time probably depends upon a combination of the directional characteristics of an aircraft as a sound source, and the position and heading of the aircraft with respect to the detector and the earth's surface.

Figure 2 also shows a short acoustic signal at 100 cps, occurring about once every 22 seconds. This signal was generated by an altitude-sensing device in the balloon-borne probe. The repetition rate of this device was inversely proportional to altitude and, for the example shown, indicates an altitude of 60,000 feet. For subsequent signature analyses the frequency generated by the altitude sensor was increased so that it would fall outside the range of the spectrometer. This was done to avoid possible confusion of altitude data with the signatures of target sounds.

Figures 3 and 4 are signature analyses from double-probe flights. The upper record is from a detector hanging close under the free-floating balloon platform. The lower record is from a second detector, hanging several hundred feet below the first. Notice that both data channels show about the same background noise level and virtually identical aircraft Doppler signatures. This indicates that the acoustic signals at the detectors were not being masked by hydrodynamic flow, and speaks well for the constant-altitude balloon as a quiet platform from which to make acoustic observations.

Figures 3 and 4 are 90-minute data samples, and therefore show a wide variety of aircraft Doppler curves and other signatures. Some of the Doppler curves show discontinuities, indicating that the aircraft changed course. Those curves which show the most rapid frequency

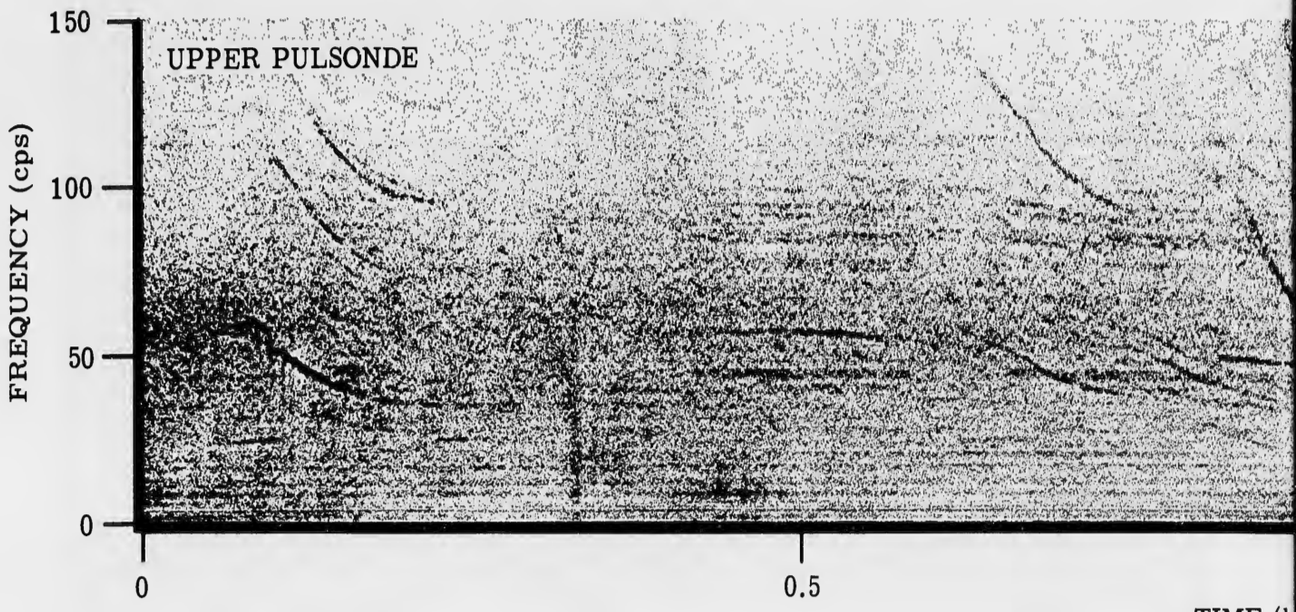

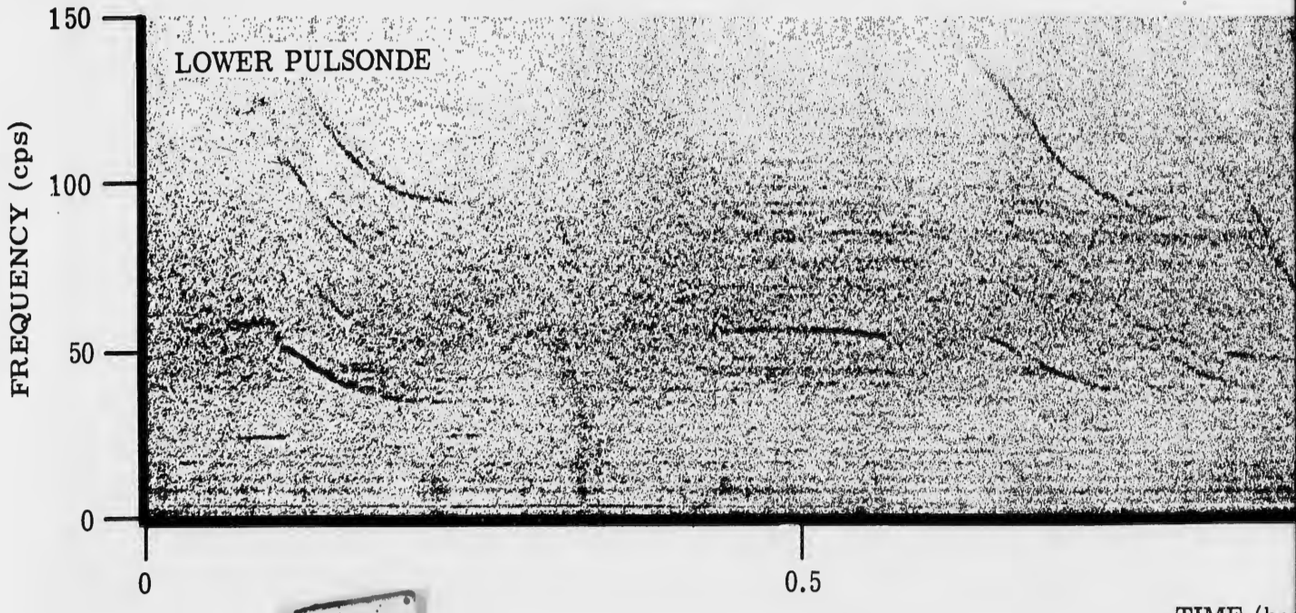

FIGURE 3. SIGNATURES FROM 2-

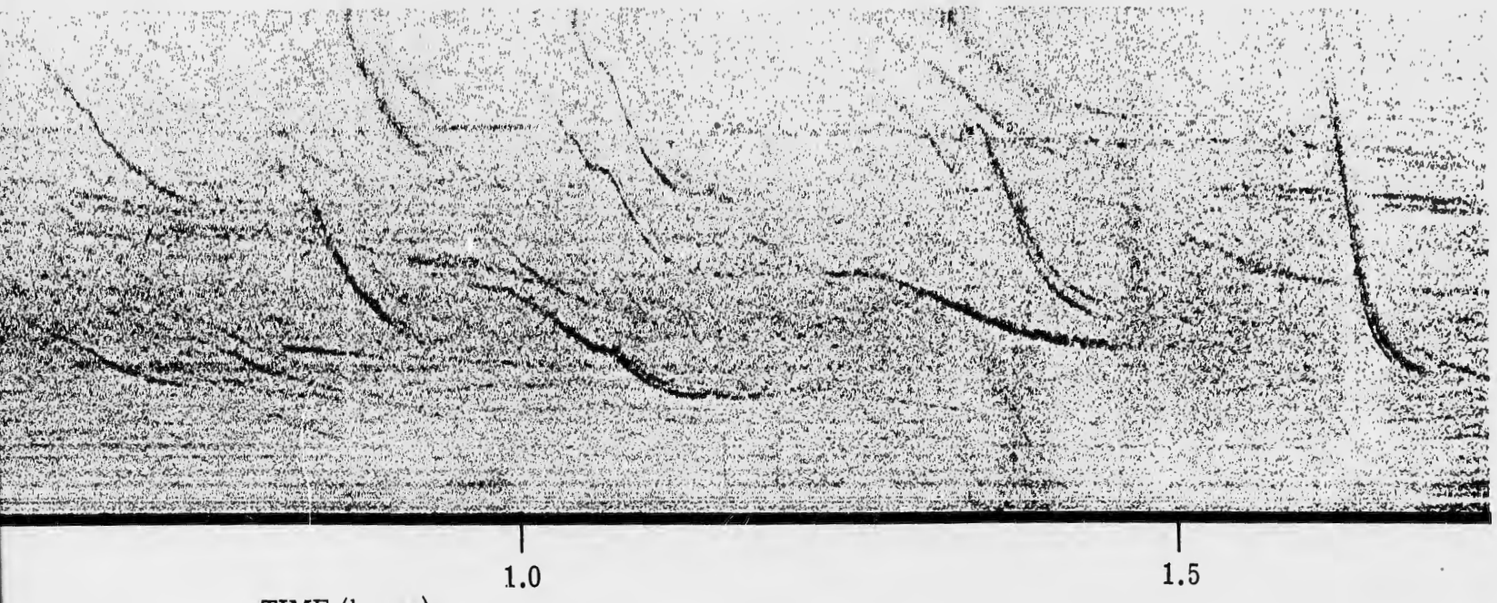

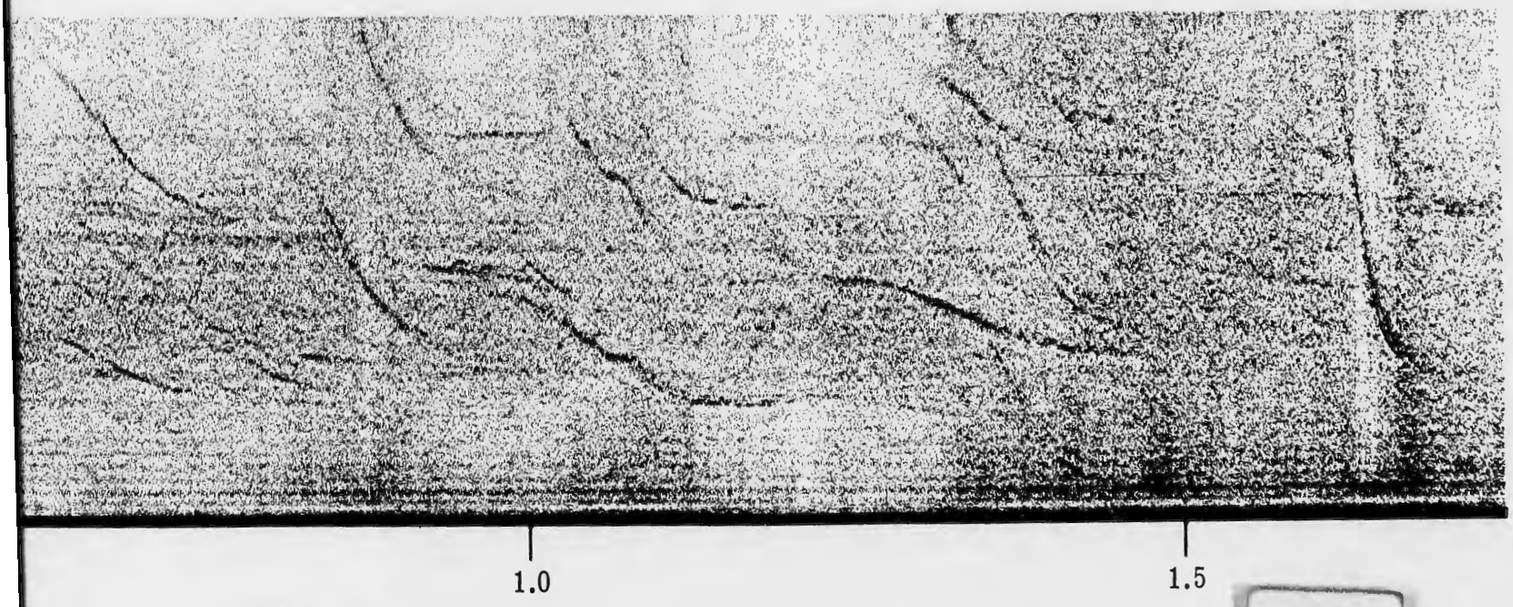

FIGURE 3. SIGNATURES FROM 2-PROBE FLIGHT OF 2-28-61

2

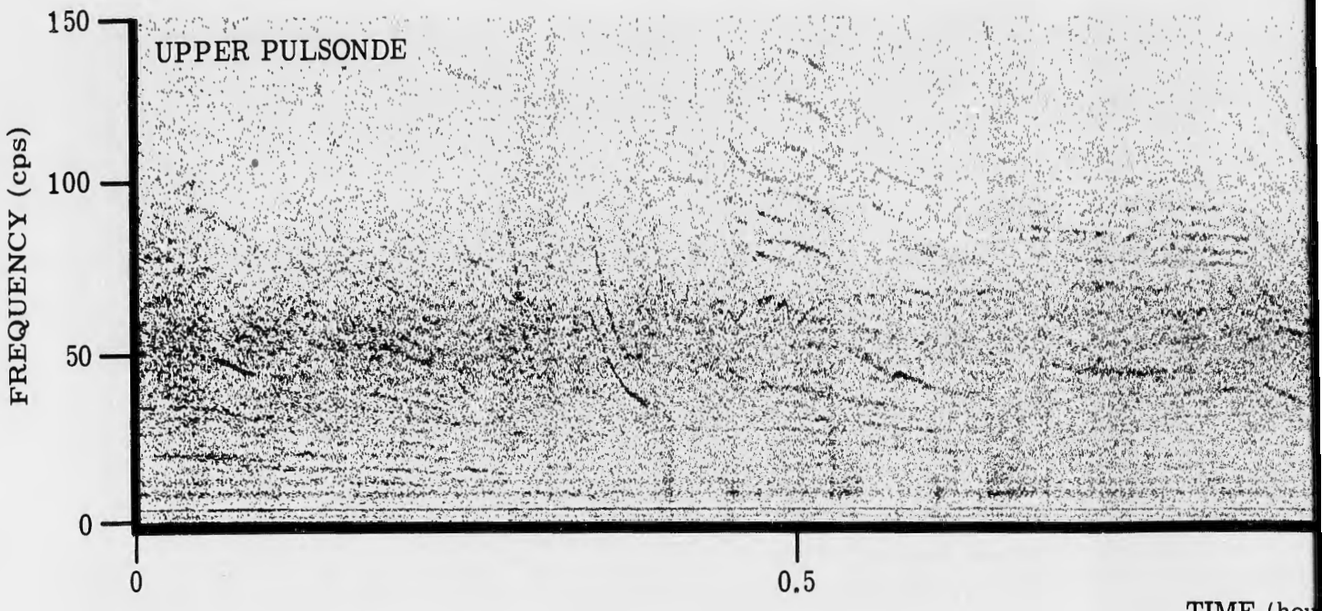

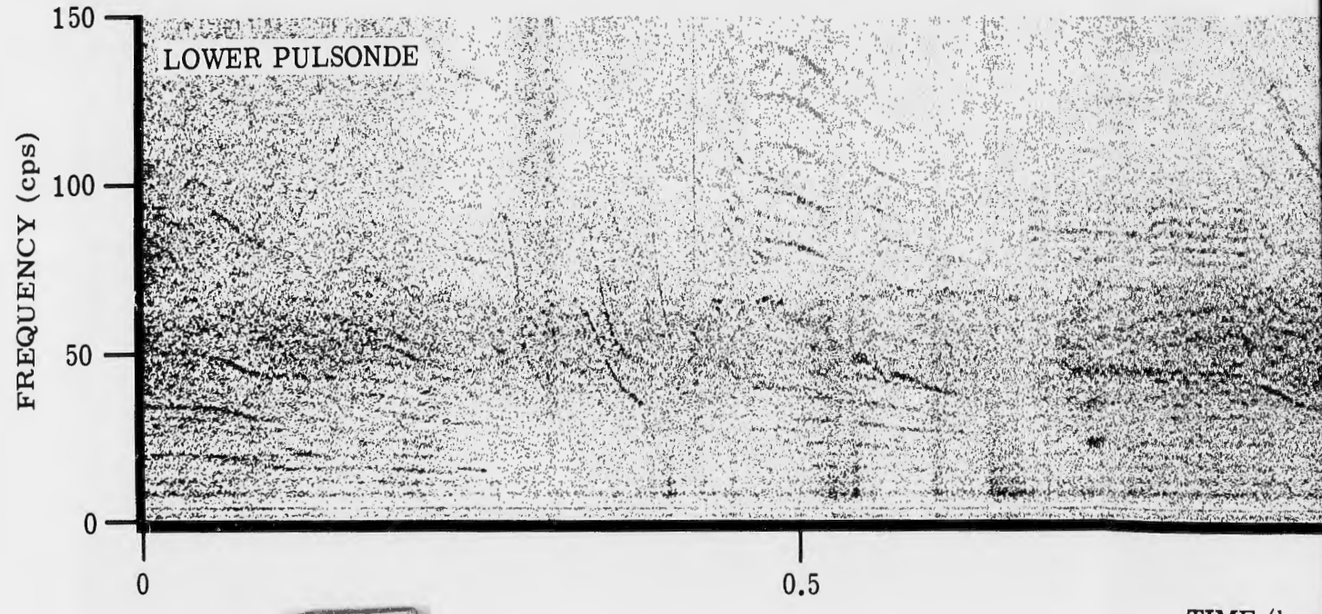

1

FIGURE 4. SIGNATURES FROM 2-PR

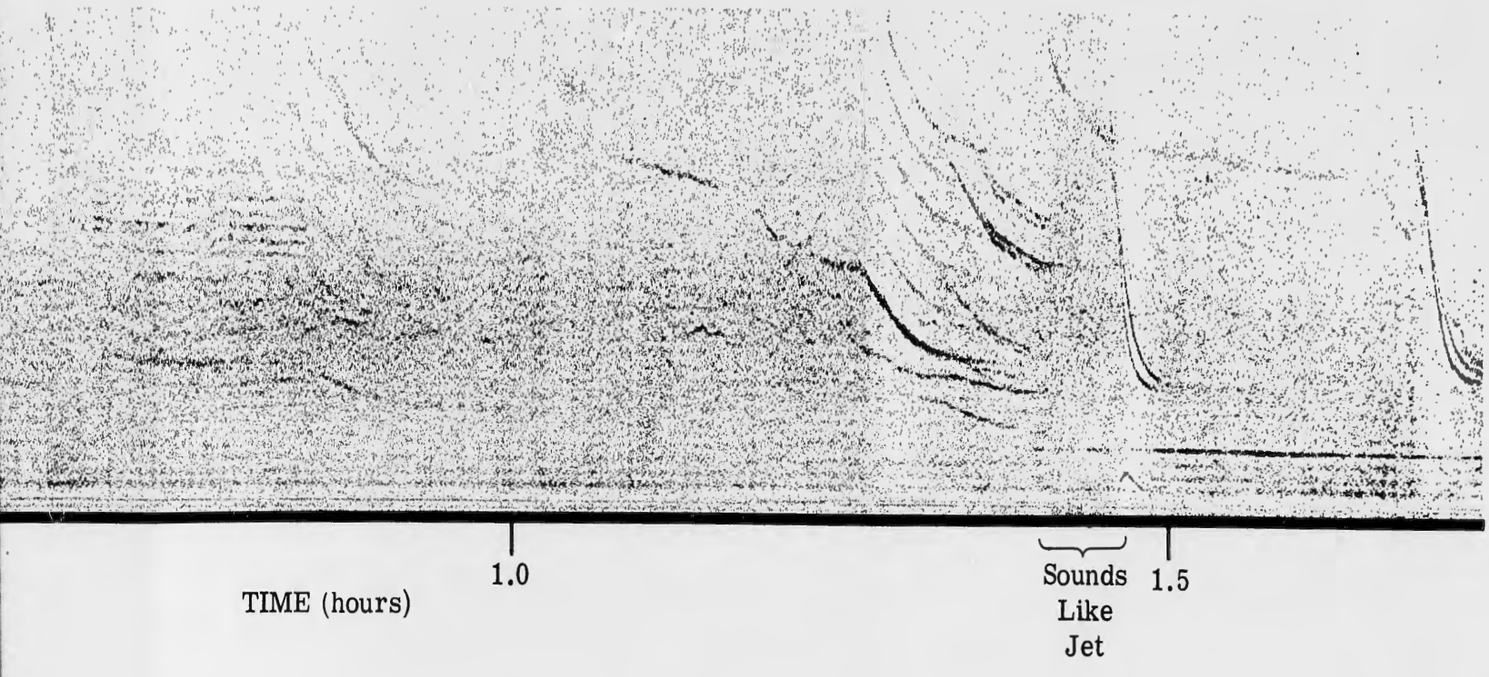

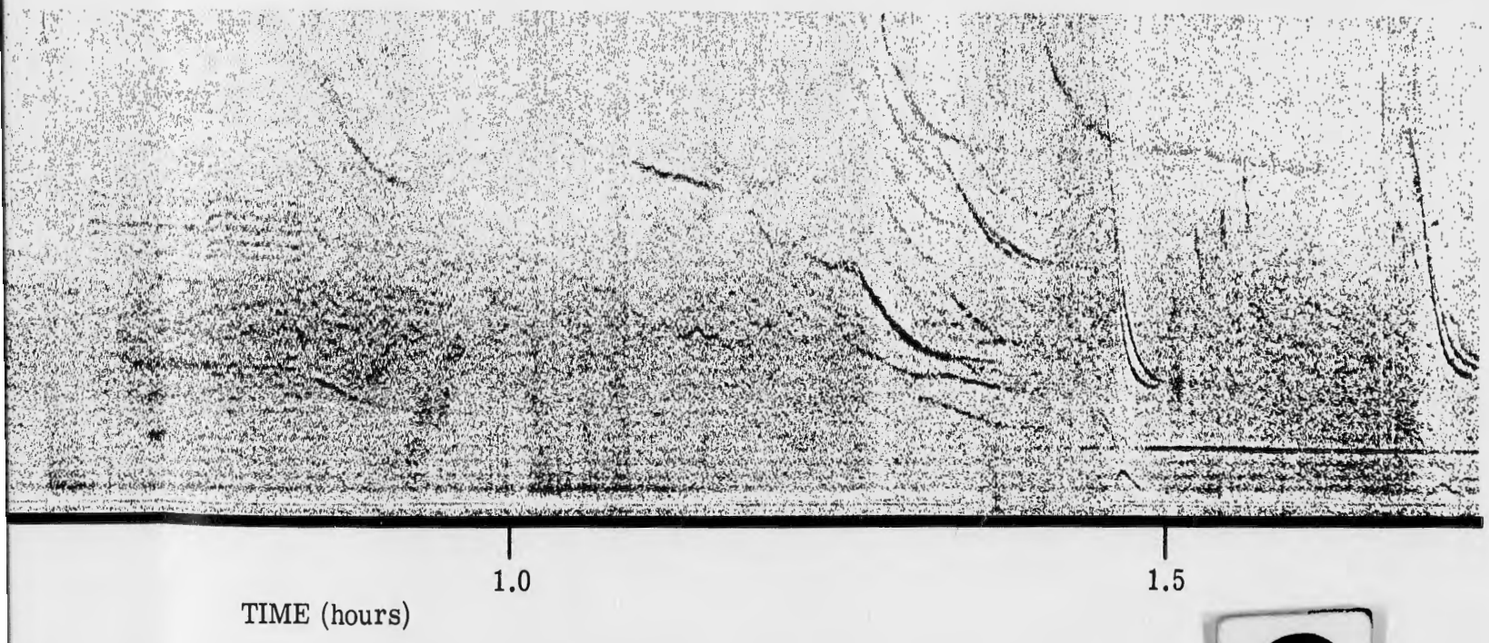

FIGURE 4. SIGNATURES FROM 2-PROBE FLIGHT OF 1-24-62

2

shifts were caused by aircraft which passed close to the detectors. Conversely, the curves showing less rapid frequency shifts were produced by aircraft which passed at longer ranges. The speed of the aircraft affects both the rate and the amount of frequency shift. Using these parameters, one can calculate not only the speed but also the passing range of any piston-engined aircraft from measurements of its Doppler signature.

Figures 3 and 4 also show the signatures of several jet aircraft; these appear as a temporary increase in broadband background noise level. The record darkens slightly for the two or three minutes that the jet is within detection range, which means that for frequencies up to 150 cps the spectrum of jet noise, though stronger, must be similar in shape to that of ambient background noise.

Figure 5 is a signature analysis of hydrodynamic noise during a double-probe balloon ascent, followed by several infrasonic events detected after the balloon reached equilibrium altitude. The frequency range of the spectrometer was set at 0 to 30 cps for this record in order to display infrasonic data in detail. The dynamic range of the instrument was set so that the darkness of the record would fluctuate between black and white for a 12-db variation in signal level. Figure 5 shows this transition occurring in approximately 1 octave during the balloon ascent, thus indicating that the spectrum of hydrodynamic noise has a negative 12 db/octave slope.

The infrasonic events shown in Figure 5 have not been identified and may be due to either natural or man-made causes. It seems unlikely that they were caused by balloon instability, because there is no measurable signal content above 5 cps. Hydrodynamic noise from balloon instability would contain frequencies above 5 cps. Infrasonic events were detected at least once, and often two or three times, an hour during summer balloon flights. During the winter the rate of occurrence dropped to once every one or two hours. The measured pressure amplitude of infrasonic events was usually about 10 dynes/cm^2. Various possible sources of infrasonic energy, one or more of which may have produced the events in Figure 5, are described in Section 4.

3.3. CROSS-CORRELATION

A cross-correlation analysis was made of the acoustic data obtained from one of several double-probe balloon flights. During this flight one acoustic detector was hung 150 feet below the other by means of a braided nylon cord. The resulting two-element array was then borne aloft by balloon to be free-floated at a constant altitude of 60,000 feet. The object was to determine whether the data sampled at 60,000 feet was propagating sound or local flow noise. Propagating sound would cross-correlate; hydrodynamic noise would not.

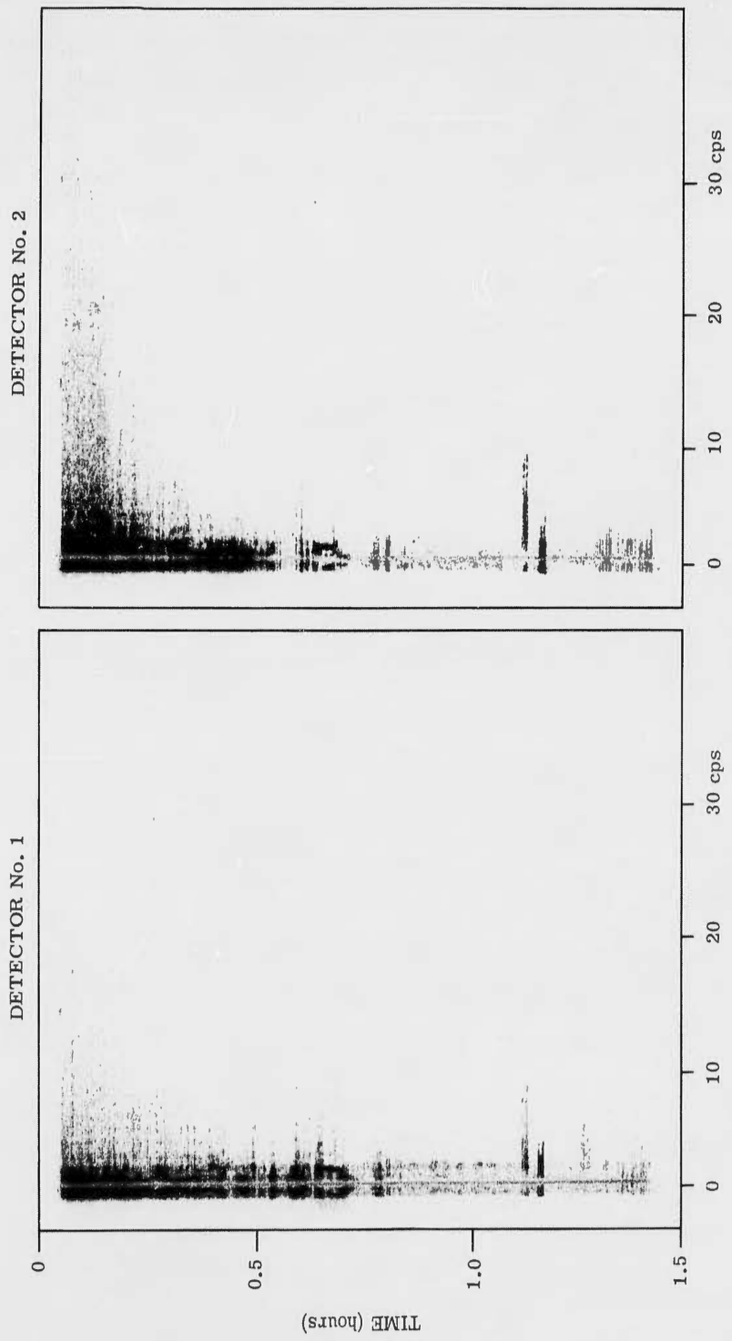

FIGURE 5. INFRASONIC EVENT CORRELATION

A magnetic-tape recording of the two data channels was cross-correlated according to the scheme illustrated in Figure 6. As the block diagram indicates, a magnetic-tape transport equipped with a special playback head stack was employed. The individual heads could be moved along the tape in relation to one another so that any desired amount of time delay (τ) between data channels could be obtained. The variable head stack is shown in Figure 7. The procedure was to set two of the heads for the time delay desired and to play the sample of recorded data. As can be seen by again referring to Figure 6, the tape playback signals were continuously multiplied together, and the product was accumulated by an integrator. This was accomplished with the electronic multipliers and integrator of a Pace Analog Computer. The process was repeated for various settings of τ. The result was displayed as a graph of normalized output from the integrator plotted against τ.

$$\phi = \lim_{T \to \infty} \frac{1}{T} \int_0^T f(t)\, g(t - \tau)\, dt$$

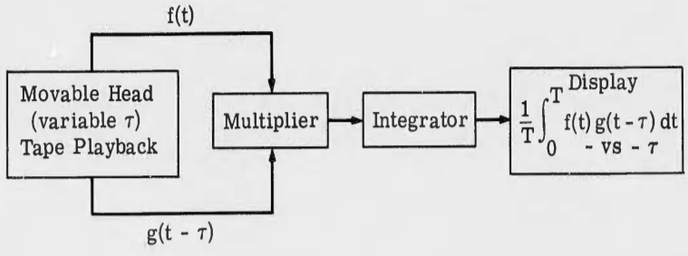

FIGURE 6. CROSS-CORRELATION PROCESS

Figure 8 shows the cross-correlation analysis for a five-minute sample of data from the double-probe flight described at the beginning of this section. A pronounced correlation of 22% occurred for a time delay between channels of 0.105 second. Microphone spacing was 150 feet for this flight, and the average speed of sound in the altitude range from 35,000 to 50,000 feet was about 1000 fps. The apparent angle from the vertical at which the correlated sound reached the microphones may then be calculated as

$$\theta = \text{arc sin} \frac{0.105 \text{ sec} \times 1000 \text{ fps}}{150 \text{ ft}}$$

$$= 45^{\circ} \text{ (approx.)}$$

From this it seems that an acoustic array placed above a plane or large volume of statistically independent noise sources, such as atmospheric shear-flow turbulence, will detect an apparent

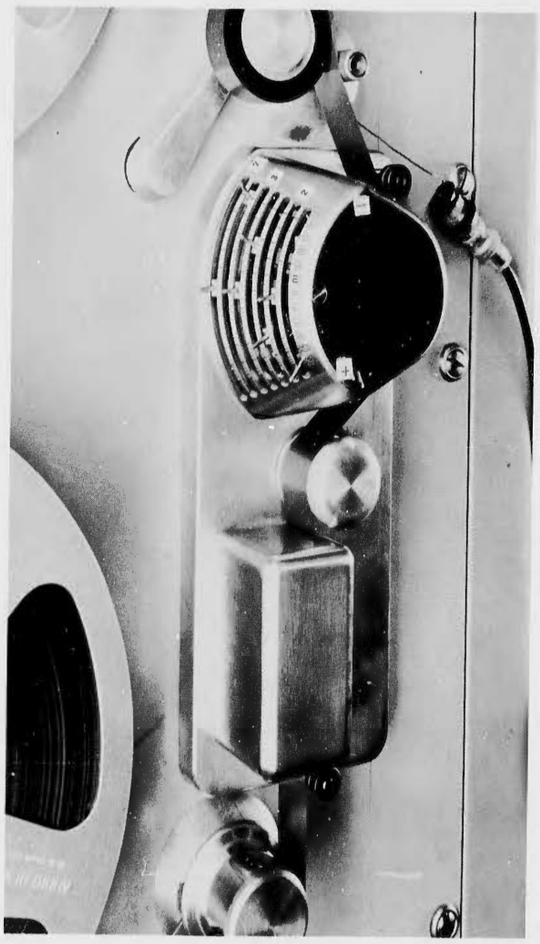

FIGURE 7. VARIABLE 7-CHANNEL HEAD STACK

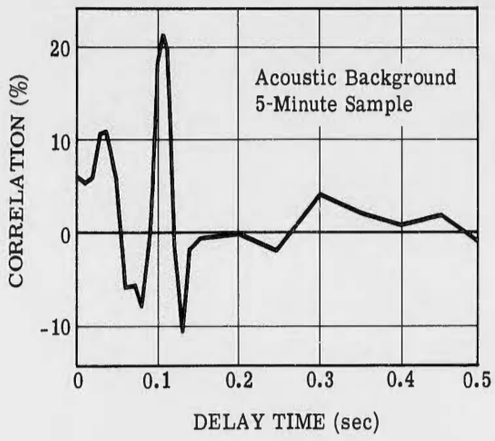

FIGURE 8. CROSS-CORRELATION 2-PROBE DATA

ring-shaped source of radius equal to the height of the array above the ring. Another way of looking at this is to say that half of the detected energy comes from within a 90^{o} solid angle, while the other half comes from outside this angle.

The bandwidth of the correlated data was from 0.2 to 30 cps. Frequencies above 30 cps were filtered out because it was found that inhomogeneities in the atmosphere around the array caused phase fluctuation in propagating sound. The amount of phase fluctuation increased with frequency for a given microphone spacing, and it was found that for ambient background noise at high altitudes, frequencies above 30 cps would not correlate. In fact, a cross-correlation index much greater than 22% could have been obtained by lowering the upper frequency limit to about 10 cps.

The cross-correlation shown by Figure 8 is proof that propagating sound rather than local flow noise was detected by the array. The value of τ for which correlation occurred shows that the sound arrived first at the lower microphone, then at the upper one. Moreover, the apparent 45^{o} angle of arrival is what would be measured if the sound were produced by a large volume or horizontal plane of statistically independent noise sources such as the turbulent eddies to be found in the atmosphere at jet stream altitudes.

3.4. PROBABILITY DISTRIBUTION

The probability distribution of amplitude for random noise is Gaussian and is given by the expression

$$P(x) = \frac{1}{\sigma\sqrt{2\pi}} e^{-x^2/2\sigma^2}$$

where P(x) = probability density, σ = standard deviation = 0.4 for random noise, and x = amplitude or pressure of the noise. The area under this curve is, by definition, unity. The expression may therefore be written as

$$\frac{1}{\sigma\sqrt{2\pi}} \int_{-\infty}^{\infty} e^{-x^2/2\sigma^2} dx = 1$$

In contrast to this, the probability density curve for a periodic function such as a sine wave is simply the reciprocal of its slope. For a sine wave, this is the secant curve with all values made positive. The curve and the area under it can be written as

$$P(x) = \frac{1}{\pi\sqrt{1 - x^2}}$$

where $1 \geq x \geq -1$

and $$\frac{1}{\pi} \int_{-1}^{+1} \frac{1}{\sqrt{1 - x^2}} dx = 1$$

Figure 9 shows the probability-density curves for Gaussian distribution and sine wave distribution as described above. They are presented here to demonstrate how dramatically different they are in shape. Meecham suggested that the shape of the probability-density curve for high-altitude background noise be determined and utilized to identify the source mechanisms [2]. He pointed out that the velocity fluctuations in hydrodynamic flow are known to be Gaussian. Since, by Bernoulli's principle, the pressure fluctuations are proportional to the square of the velocity fluctuations for hydrodynamic flow, the probability distribution of pressure should be non-Gaussian. In fact, the probability distribution of pressure for flow noise should lie on a curve having much steeper sides than the Gaussian curve.

On the other hand, the probability distribution of pressure for the far-field noise from turbulence should be Gaussian, because the propagating sound field is made up of contributions from a large number of randomly distributed and statistically independent sound sources—the turbulent eddies produced by wind shear around the jet stream.

Probability-density curves for flow noise and for high-altitude background noise were prepared from samples of tape recorded data. The sample of flow noise was obtained during the ascent phase of a balloon flight. The measured ascent rate was about 700 fpm, equivalent to an 8-mph wind blowing past the acoustic probe. The sample of background noise was obtained later on during the same flight, after the balloon had leveled off and was free-floating at a constant altitude of 60,000 feet. Oscillograms showing the waveforms of both data samples were obtained. The upper frequency limit of these oscillograms was held to 10 cps to control the maximum slope of the record for the fastest oscillograph-paper speed that was available.

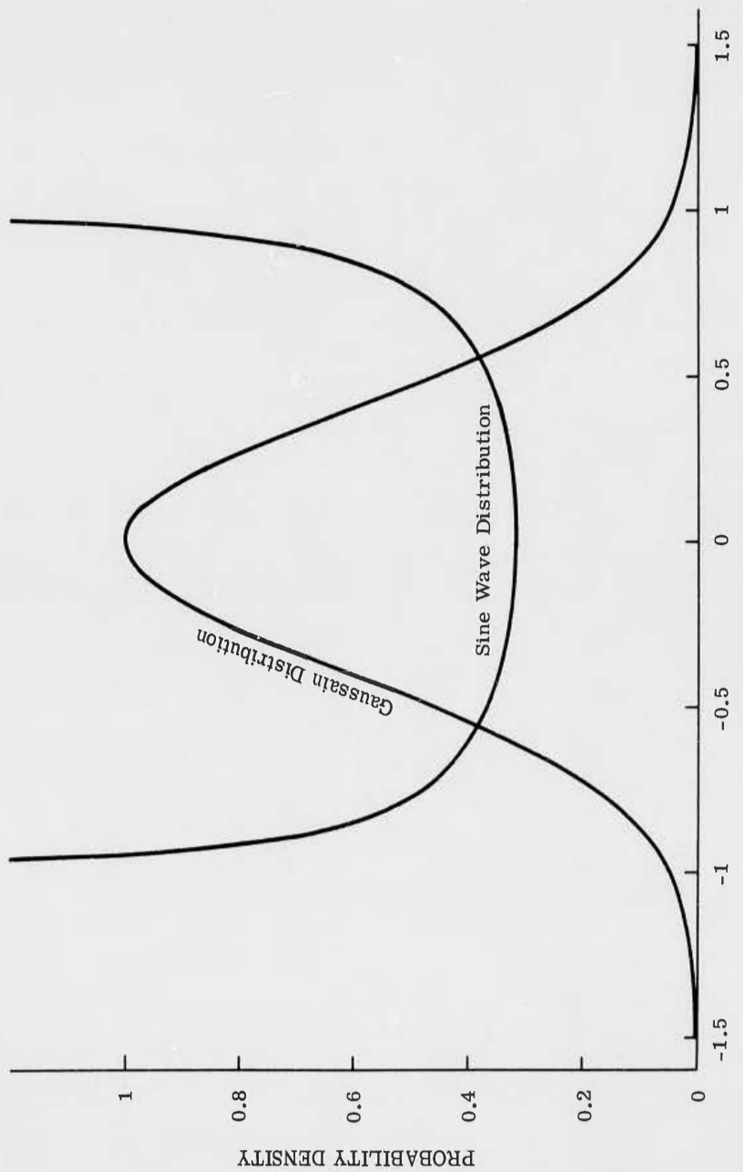

FIGURE 9. GAUSSIAN AND SINE WAVE PROBABILITY DISTRIBUTIONS

The oscillograms were made on paper that was preprinted in rectangular coordinates. The time base was marked off in increments of 0.02 seconds, and the amplitude range (proportional to acoustic pressure) was ±5 cm, marked off in 1-mm increments. A 40-second segment of each oscillogram was then processed to provide data for plotting probability-density curves.

At each time increment of 0.02 seconds along an oscillogram the amplitude was measured to the nearest millimeter. A table was prepared, listing how many times the amplitude of the oscillogram was at each incremental level. A curve for amplitude vs. number of readings was then plotted. Finally, the curve was normalized by making its peak equivalent to unity. The result was an empirically determined probability-density curve.

Figure 10 shows probability-density curves for flow noise and for high-altitude ambient background. The curves were prepared in the manner described above. A Gaussian distribution curve is shown for reference. The distribution curve for flow noise is much steeper than Gaussian and, in fact, closely resembles an $e^{-\left|\frac{x}{2\sigma^2}\right|}$ curve in contrast to the Gaussian $e^{-\frac{x^2}{2\sigma^2}}$. The curve for ambient background, however, is very nearly Gaussian, apparently even broader than Gaussian. Thus the measured distribution curves more than bear out the theoretical predictions made at the beginning of this section. The experimental results indicate that high-altitude background noise is not flow noise, but is probably sound radiated from a random distribution of independent sources, such as turbulent eddies.

4
TECHNICAL DISCUSSION

In this section the various natural sources of infrasonic energy in the atmosphere are discussed. Most of these sources can produce a quasi-time-steady acoustic background level for periods from several minutes up to many hours. Atmospheric turbulence as a source of sound is discussed in detail because it is considered the principal contributor to ambient acoustic noise at high altitudes. Identifying characteristics of the sounds produced by other natural sources are described. By virtue of these characteristics it should be possible to distinguish the far-field noise of atmospheric turbulence from noise produced by other natural sources.

4.1. ATMOSPHERIC TURBULENCE

A fundamental paper on the local structure of turbulence was published in 1941 by A. N. Kolmogoroff [4]. The bulk of experimental evidence from wind tunnel, jet exhaust, and meteorological measurements supports Kolmogoroff's physical and mathematical concept of turbulent

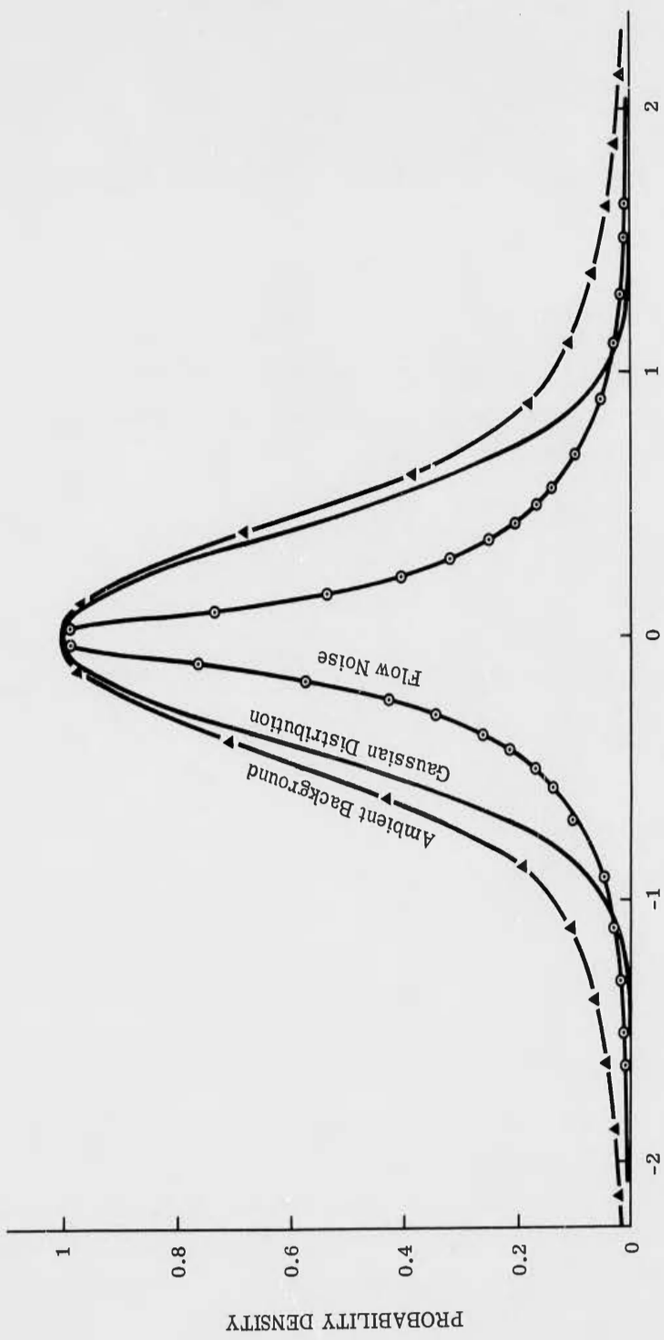

FIGURE 10. AMBIENT BACKGROUND AND FLOW NOISE PROBABILITY DISTRIBUTIONS

structure. Kolmogoroff supposes that there are three ranges of eddy sizes in a turbulent system. In the first range, energy is supplied to the turbulence by the generation of very large eddies. Such eddies would be generated in free atmosphere by wind shear action above, below, and on either side of a jet stream core. The largest eddies are characterized by a dimension L.

In the second range of turbulence, the large eddies decay and in the process generate somewhat smaller eddies. In turn, the somewhat smaller eddies decay while generating still smaller eddies, and so on. Because of this action, the shape of the energy spectrum of the second range of turbulence, known as the inertial subrange, is independent of the driving forces that generated the largest eddies. In fact, the energy spectrum, E(k), for the inertial subrange based on Kolmogoroff's similarity hypothesis, depends only upon ϵ, the amount of power per unit of mass in the medium that produces the turbulence, and upon k, the wave number of the turbulent pressure fluctuations. Thus

$$E(k) = \epsilon^{2/3} k^{-5/3}$$

is the energy spectrum of turbulence in the inertial subrange. This is often referred to as the 5/3 law. While this "law" has still not been proved conclusively, it is widely accepted because of the growing amount of experimental evidence that supports it. In the case of atmospheric turbulence, supporting evidence for the 5/3 law was obtained recently by MacCready, using a sailplane equipped with an accelerometer and hot-wire anemometer [5, 6].

In the third range of turbulence, eddy sizes are very small and fluctuations are very rapid, though of small amplitude. The velocity fluctuations are so rapid, in fact, that viscous effects in the medium quickly dissipate all remaining turbulent energy as heat. Thus, in summary, a large-scale motion or flow in a medium such as the atmosphere energizes large eddies. This energy cascades through the inertial subrange at a rate of ϵ per unit mass while producing progressively smaller but more rapidly fluctuating eddies. Finally, the energy transported to the smallest eddies is dissipated in heat because of the viscosity of the medium.

Formulas utilizing Kolmogoroff's inertial subrange concept have been developed by Meecham and Ford [3]. These formulas describe the acoustic power spectrum of sound radiated by turbulence. The proportion of turbulent energy that is converted into acoustic energy is very small. On the other hand, these small amounts of acoustic energy propagate as sound waves and, in the case of atmospheric turbulence, have been detected at ranges of many miles from the the source [1, 7]. Thus, the shape of the acoustic power spectrum of turbulence-generated noise should help to identify this type of noise from other sounds in the atmosphere.

Meecham and Ford calculate the acoustic power spectrum for the first range, where the largest eddies are being produced, as

$$P(\omega) \sim \rho_0 \, Vc_0^{\,2} \, M^3 \left(\frac{\omega L}{c_0}\right)^4$$

where ρ_0 is the mean density, V is the volume considered, c_0 is the local speed of sound, M is the turbulence Mach number, $\omega = 2\pi f$, and L is the size of largest eddies. Stated simply, the acoustic power radiated by the largest eddies is proportional to the fourth power of frequency.

For Kolmogoroff's inertial subrange, Meecham and Ford calculate the acoustic power spectrum to be

$$P(\omega) \sim \rho_0 Vc_0^{\,2} M^{21/2} \left(\frac{\omega L}{c_0}\right)^{-7/2}$$

where the symbols have the same definitions as above. In other words, the amount of acoustic power per cycle of bandwidth in the inertial subrange falls off as the 7/2 power of frequency. For the third range there is very little acoustic energy radiated since most of the energy is dissipated in heat.

From the preceding discussion one can now draw a simple graph for the power spectrum of sound radiated by turbulence. The significance of this graph is that the power spectrum curves for the first and second ranges of turbulence intersect at a frequency of $\omega = \frac{Mc_0}{L}$. This means that by using a spectrum analyzer one can find the frequency ω at which the energy peaks and can thus determine $\frac{Mc_0}{L}$. The turbulence Mach number, M, can be estimated for high-altitude turbulence from balloon-tracking data. Now, calculating the local speed of sound, c_0, from temperature measurements, one can calculate the size, L, of the largest turbulent eddies.

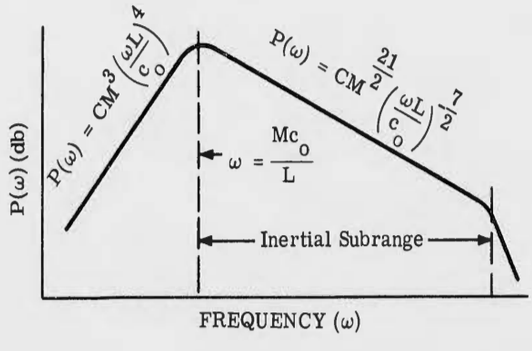

In studying upper-air turbulence as a source of acoustic background noise in the atmosphere, it will be important to determine the frequency, ω, where the large eddies initiate the inertial subrange. If this frequency is found to shift only slightly with diurnal changes in turbulence Mach number and large-eddy size, it could then be utilized as a key or characteristic signature for identifying turbulence noise. MacCready [6, 8], Press [9], Saunders [10], and Batchelor [11] make various estimates of large-eddy size at high altitudes for the inertial subrange. Eddy sizes of from 100 to 300 meters fall within their estimates. For turbulence Mach numbers of 0.1 to 0.2, the low-frequency end of the acoustic radiation should then peak at about 0.1 cps.

4.2. OCEAN WAVES

Waves on the surface of the ocean may be thought of as a mixture of very slow traveling waves and random fluctuations of the sea surface. The slow wave trains, traveling at much less than the speed of sound, produce a self-cancelling sound field, but the random fluctuations radiate sound into the air. This type of radiation is somewhat similar to that from high-altitude turbulence. Daniels likens the ocean surface to an infinite plane made up of pistons, roughly 40 meters square, oscillating in random phase at a frequency of 0.2 cps [12]. In drawing this picture, Daniels is referring specifically to the random component of surface fluctuations. He reports maximum acoustic pressures of 6 dynes/cm^2 having a predominant frequency of 0.2 cps as measured at Ft. Monmouth, N. J. He relates this measurement to a small tropical hurricane a few hundred miles off the New Jersey coast. Finally, he accredits the long range propagation of sound from ocean waves to refractive ducting in the atmosphere.

More recently, Cook and Young [13] report measurements that agree with those of Daniels. They report acoustic pressures of 1 and 2 dynes/cm^2 as being typical, and pressures of 6 dynes/cm^2 as indicating storms off the Atlantic coast. They also report predominant frequencies of about 0.2 cps. At their monitoring station in Washington, D. C., they measure these sound waves as traveling parallel to the earth's surface and coming mainly from an easterly direction. On the west coast of the U. S., some of the earliest measurements of sound from ocean waves were made by Benioff and Gutenberg in 1939 [14]. Their measurements indicated maximum acoustic pressures of 6 dynes/cm^2 and average pressures of 1 dyne/cm^2 at frequencies of about 0.2 cps for waves traveling at the speed of sound and coming from the Pacific Ocean. They called these sound waves "microbaroms" because of their analogy to "microseisms." Both phenomena have predominant frequencies of about 0.2 cps.

From the foregoing discussion it should be possible to distinguish the microbaroms, caused by ocean waves, from the sound generated by upper-air turbulence. Spectrum analysis would reveal the near-sinusoidal character of microbaroms at a frequency of about 0.2 cps. The

theoretical power spectrum of turbulence noise, as discussed earlier, falls off as the 7/2 power of frequency in the inertial subrange. Moreover, the sound of high-altitude turbulence will be detected by an acoustic array as propagating from jet stream altitudes. Microbaroms are reported as propagating horizontally from nearby large bodies of water. Finally, one would expect turbulence noise to predominate over microbaroms for inland areas, and microbaroms to predominate over turbulence noise for coastal areas, at least during off-shore storms.

4.3. SEISMIC WAVES

There is some evidence that seismic events of magnitude 5 and larger couple detectable amounts of acoustic energy into the atmosphere. Cook and Young show impressive oscillograms of signals recorded from four low-frequency microphones operated as an array by the National Bureau of Standards in Washington, D. C. [13]. These oscillograms agree closely with those recorded from seismometers by the Coast and Geodetic Survey in Washington. The event recorded was the Montana earthquake of 1959. The acoustic signals in Washington were reportedly generated by earth motions that resulted from seismic energy arriving in Washington from Montana. The first P wave on the acoustic records is partially obscured by local wind noise and microbaroms. The first S wave is well above local background noise, as are several multipath arrivals of reflected P and S waves. The Rayleigh or surface waves are very strong, and Cook and Young report that the corresponding sound pressures generated in Washington were about 3 dynes/cm^2 peak-to-peak. The highest frequencies recorded (above microbarom levels) appear to be about 0.125 cps.

Cook and Young's results have been reinterpreted by other investigators, who suggest that the microphones used were, in effect, geophones. This implies that the microphone diaphragms were held almost stationary by coupling to the atmosphere, and that the microphone frames were deflected by earth motion. In any case, it appears that infrasonic microphones respond in some way to seismic activity, and that the resulting electrical signal level at the microphone terminals is significant, whether caused by acoustic pressure fluctuations or by motion of the microphone itself.

It should be possible to distinguish between seismic and acoustic signals as detected with infrasonic microphones. One obvious way would be to operate a seismometer in the same area with the acoustic detection system and compare results. Another way would be to examine the pattern of signals received for the characteristic P, S, and Rayleigh waves that propagate from seismic events. Still another way would be to measure the speed of propagation across a ground-based array. For seismically caused signals, this will be at least an order of magnitude faster than for an acoustic wave that has propagated from a distant event.

4.4. MAGNETIC STORMS

Corpuscular radiation from the sun increases erratically during solar flares. Particles traveling along curved paths at speeds of 1000 to 3000 km/sec reach our ionosphere about 1 1/2 days later and produce plasma clouds. These clouds perturb the earth's magnetic field and cause geomagnetic storms. Magnetohydrodynamic waves are generated by the interaction of the storms with plasma. Some of the energy in these waves is converted to infrasound by the outer atmosphere, and propagates to earth. Because of the steep angles of arrival, horizontal trace velocities of Mach 2 and greater are measured. Frequencies of 0.005 to 0.05 cps and acoustic pressures of 2 to 7 dynes/cm^2 are reported by Cook and Young [13]. It should be easy to identify this type of infrasound by its unusually low frequencies and high trace velocities. Moreover, this signal usually persists for at least several hours.

4.5. HURRICANES, TORNADOES, METEORS, AND LIGHTNING

Hurricanes, tornadoes, meteors, and lightning bolts generate acoustic energy, some of which is in the infrasonic range. Acoustic signals received at long ranges from these events should propagate at the local speed of sound. The signals from hurricanes and tornadoes should persist from a half-hour to several hours. The signals from meteors and lightning bolts, which begin as shock waves, should be comparatively brief. In the case of lightning bolts, the signal might be expected to persist briefly and at random intervals, in the manner characteristic of a thunderstorm.

5
EQUIPMENT

5.1. PULSONDE ACOUSTIC SENSOR

Acoustic background at high altitudes was monitored with a balloon-borne, battery-powered, infrasonic-microphone, uhf-radio-transmitter package known as the Pulsonde Acoustic Sensing Device. This was developed jointly by personnel at the U. S. Army Electronic Research and Development Activity, White Sands, New Mexico [15] and at Schellenger Research Laboratory of Texas Western College [16, 17]. Figure 11 is a view of a Pulsonde which has been partly disassembled in order to display its infrasonic capacitor microphone and Radiosonde-type transmitter. Also shown is a water-activated battery which will operate the Pulsonde for a continuous period of 10 hours. Figure 12 is a view of a Pulsonde that has been entirely removed from its cardboard container in order to show a barometrically operated altitude-sensing device. The Pulsonde microphone, its amplifier, the altitude sensor circuit, and the pulse modulation circuit were built around a modified AN/AMT-4A Radiosonde transmitter [18] so that an

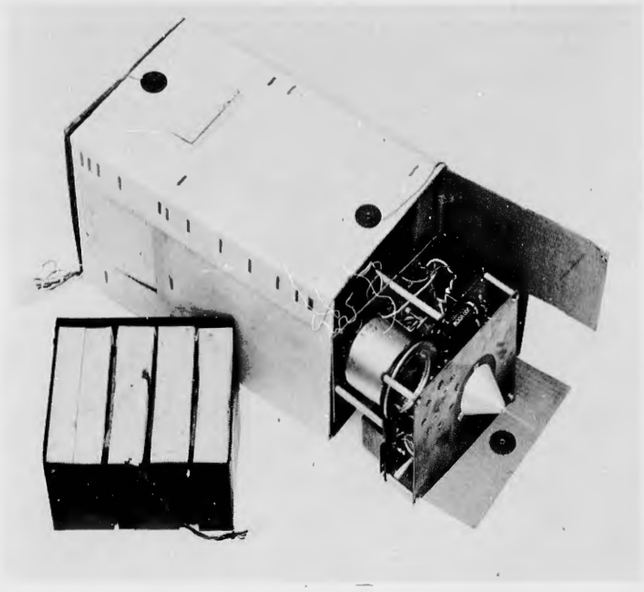

FIGURE 11. PULSONDE ACOUSTICAL SENSOR

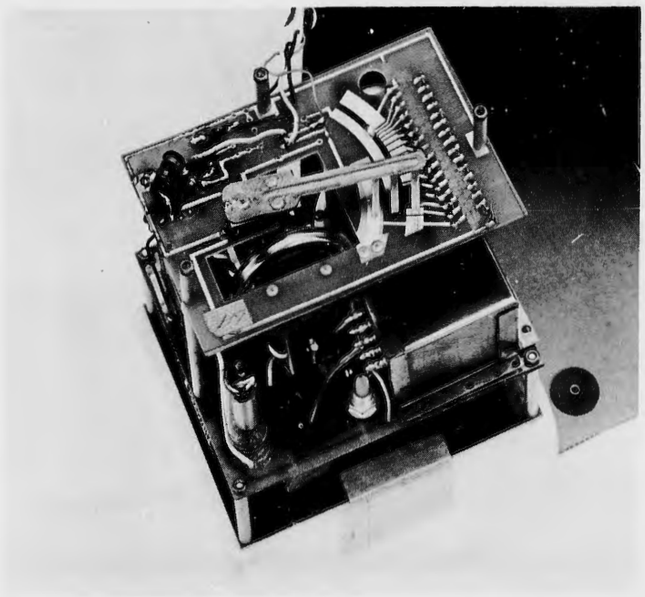

FIGURE 12. PULSONDE ALTITUDE SENSOR

AN/GMD-1A Rawin Set [19] could be used to track the Pulsonde and receive the acoustic and altitude data transmitted by it. Just before each Pulsonde was launched, the gain of its microphone amplifier was set so that at a frequency of 5 cps the received and demodulated signal level would be 1 volt for an input sound pressure of 1 dyne/cm^2. A preemphasis network of 6 db/octave in the microphone amplifier compensated for the anticipated shape of the background noise spectrum. Therefore the system's sensitivity became progressively greater for frequencies above 5 cps.

5.2. TRACKING VAN

An AN/GMD-1A Rawin Set mounted in a military van tracked the Pulsondes and received the data on which this report is based. Figure 13 is an exterior view of the van, showing the GMD tracking antenna on the roof. Actually the antenna is mounted on an elevator platform which can be lowered from the roof to the floor of the van for highway travel. On top of the tracking-antenna dish an auxiliary Yagi antenna is mounted. The Yagi antenna can be used to transmit a ranging signal to a special type of Radiosonde, which receives the ranging signal and retransmits it back to the tracking van.

Figure 14 is an interior view of the van. Range, elevation angle, and azimuth angle to the target (Pulsonde or Radiosonde) are continuously displayed and printed out by the equipment bay on the right. The second bay from the right contains a demodulator for Pulsonde data (top of bay); an audio amplifier, which drives a loudspeaker for monitoring acoustic data; and meteorological readout equipment for recording temperature, humidity, and altitude data from Radiosondes (bottom of bay). The third bay from the right contains a seven-channel FM tape recorder, which records Pulsonde data that has been received and demodulated. The tapes can then be replayed and processed later in the laboratory. A microphone and preamplifier are included at the bottom of the tape-recorder bay for placing voice commentary on one of the tape channels. The bay on the left contains a constant-frequency, motor-drive amplifier for the tape recorder, and an oscilloscope for checking circuits and monitoring waveforms of incoming data.

A second GMD receiver and a dual-channel PFM discriminator were installed in another part of the van so that data from double-Pulsonde balloon flights could be acquired for the cross-correlation experiment. A block diagram of the two-channel receiving system that was developed for the cross-correlation experiment is shown in Figure 15. The feature of the system is that it requires only one high-gain, automatic-tracking antenna. Advantage is taken of the fact that two different i-f's can be developed by one local oscillator and mixer circuit by merely tuning the Pulsonde transmitters to slightly different frequencies. The frequencies chosen were 1680 and 1695 Mc, both of which fall within the operating range of the AN/GMD-1A tracking antenna. A circuit diagram of the dual-channel PFM discriminator developed for this system is given in Figure 16.

FIGURE 13. TRACKING VAN, EXTERIOR VIEW

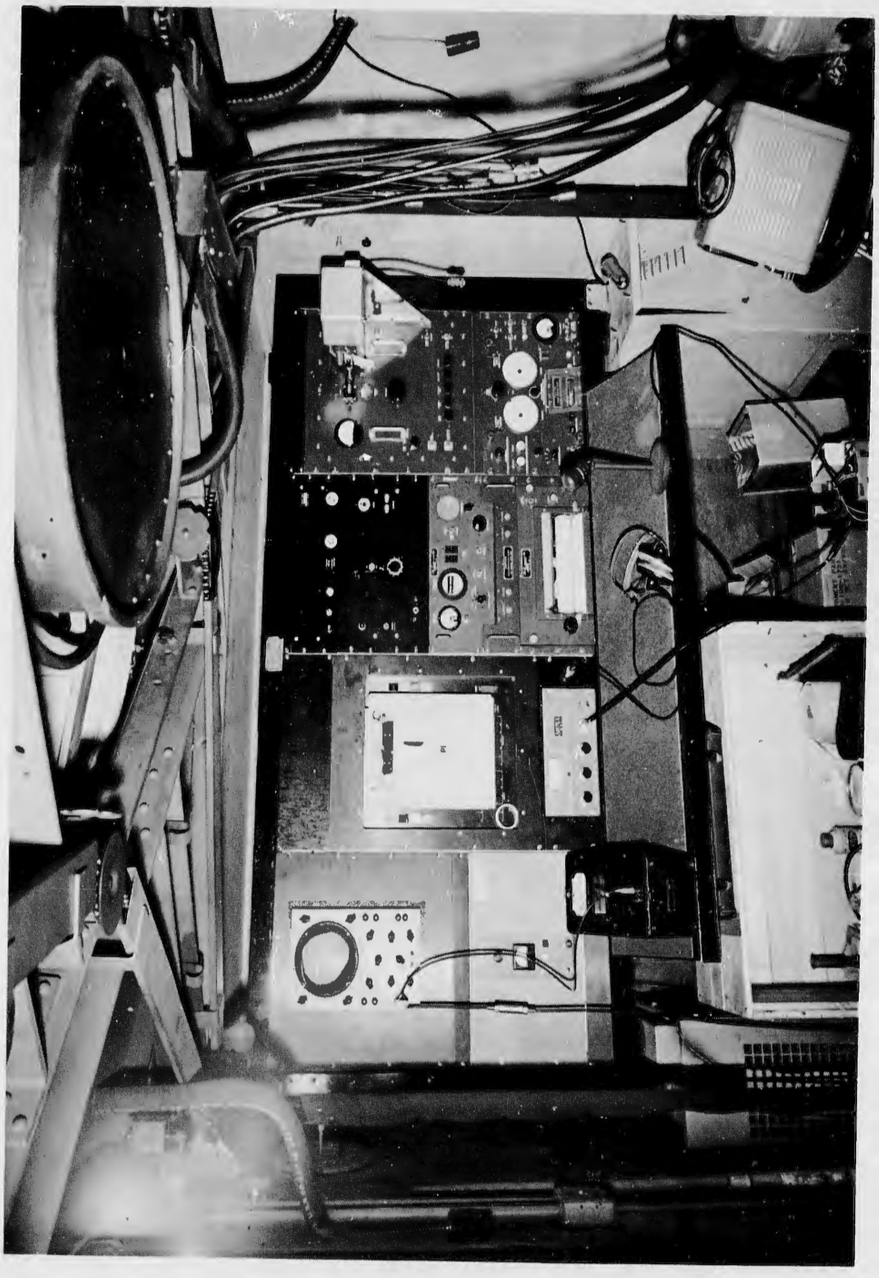

FIGURE 14. TRACKING VAN, INTERIOR VIEW

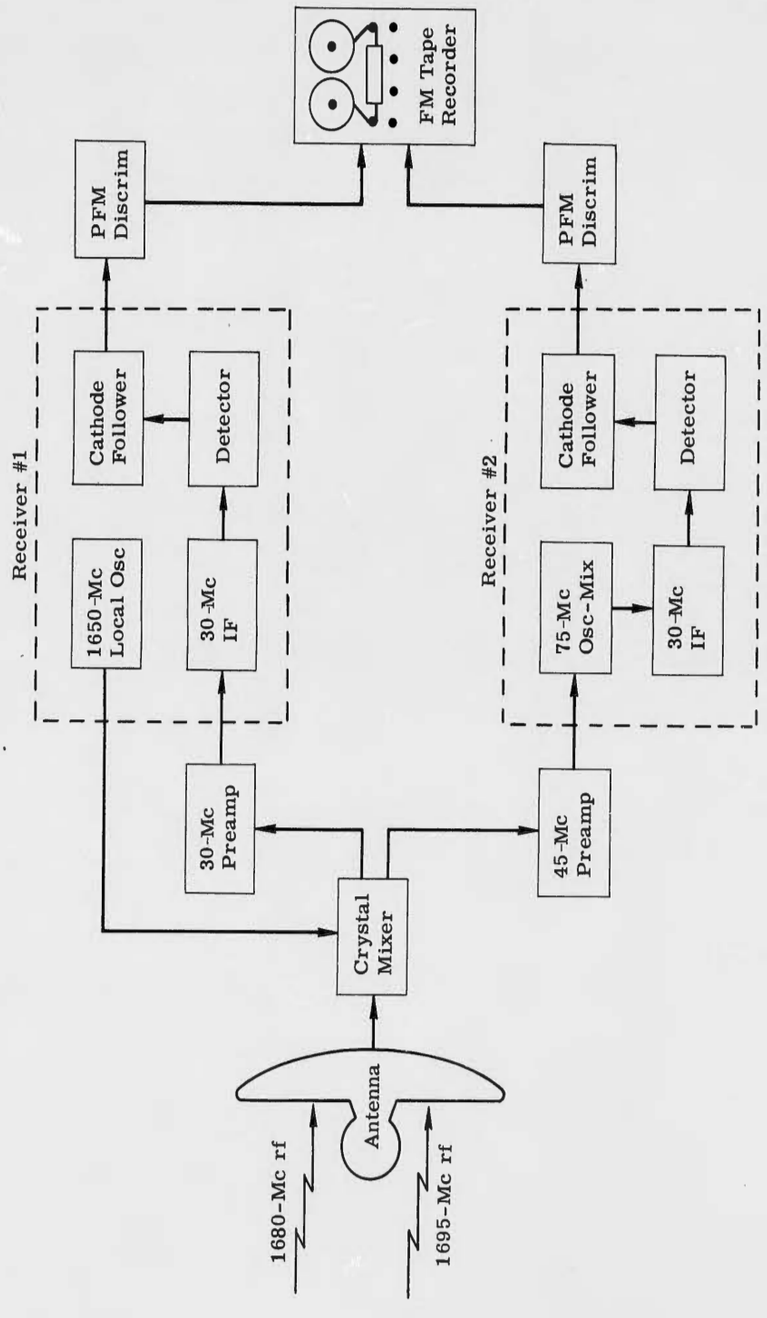

FIGURE 15. BLOCK DIAGRAM, 2-CHANNEL RECEIVING SYSTEM

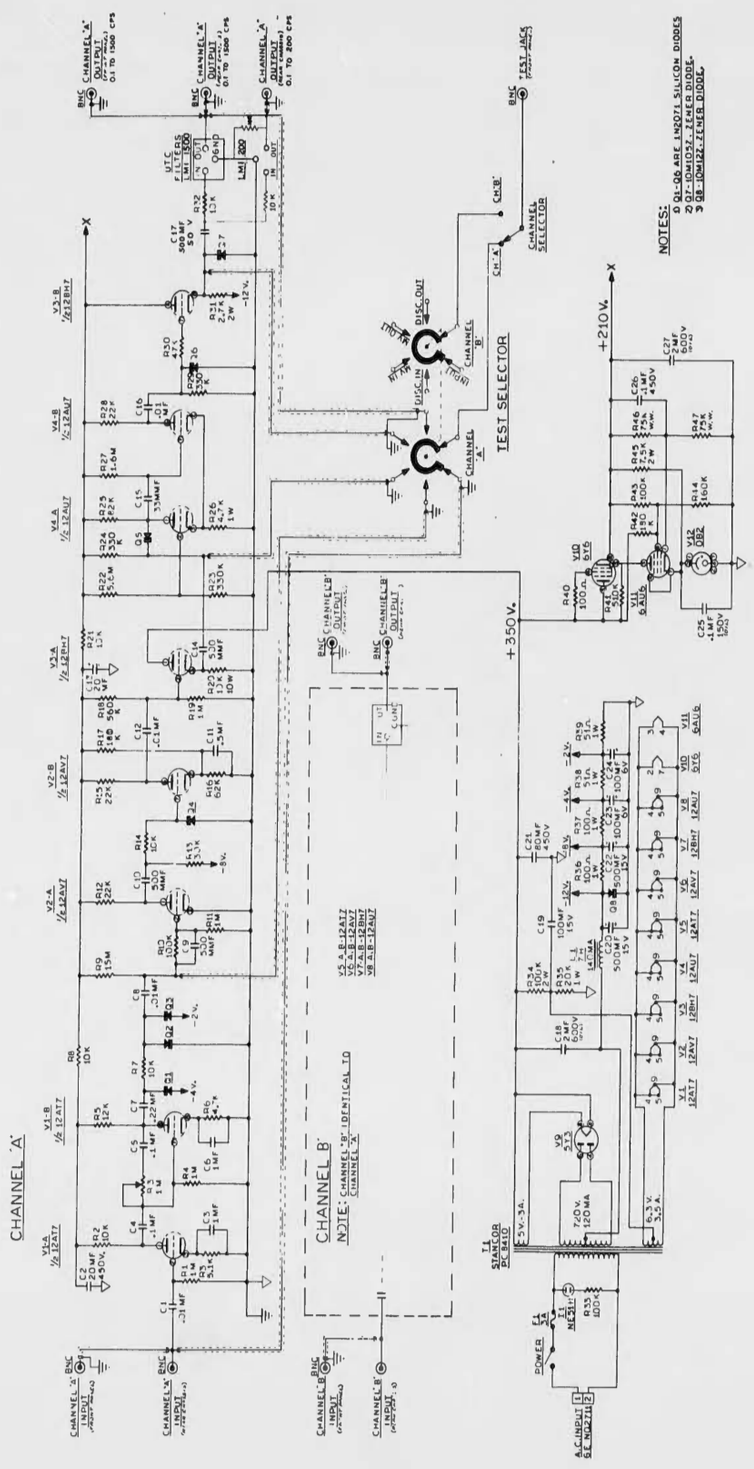

FIGURE 16. CIRCUIT DIAGRAM OF PFM DUAL-CHANNEL DISCRIMINATOR

5.3. PISTONPHONE CALIBRATOR

A pistonphone was developed for calibrating Pulsonde microphones and overall system response. The pistonphone features pushbutton selection of frequencies at one-octave intervals from 0.125 to 30 cps, and a sealed diaphragm type of piston to eliminate air leaks. Although this instrument was developed to calibrate Pulsonde acoustical sensors, it would serve equally well for calibrating any type of infrasonic sensor.

The pistonphone chamber consists of nothing more than a large bell jar lying on its side with a 1/2-inch thick aluminum plate clamped across its mouth. A hole in the plate is sealed with a flexible diaphragm that is deflected in and out by a rod that connects to an eccentric drive. The eccentric drive operates from a gearbox equipped with pushbutton gear selectors. The gearbox is driven by a synchronous motor. Both are shock-mounted on the thick aluminum plate. The bell jar is about 18 inches in diameter and 30 inches long. The incremental volume change caused by the flexing diaphragm produces a pressure fluctuation of 10 dynes/cm^2 rms inside the sealed bell jar under standard atmospheric conditions.

Figure 17 is a photograph showing the pistonphone pushbutton frequency selector. Note that frequencies are available at one-octave intervals from 0.125 to 30 cps. The synchronous motor drive is shown mounted directly beneath the frequency-selector panel. Figure 18 is another view of the pistonphone, showing the flexible diaphragm, connecting rod, and eccentric drive, isolated from gearbox and motor vibrations by two flexible couplings. Also shown in Figure 18 are a vacuum pump and mercury manometer used to simulate high-altitude air pressures by pumping part of the air out of the bell jar.

Figure 19 is a detailed view of the flexible diaphragm, connecting rod, and eccentric drive. The diaphragm was cut from a sheet of 0.01-inch-thick Teflon and sealed over a hole in the thick aluminum plate with a clamping ring and eight bolts, as shown. The diaphragm is clamped at the center between two large round washers. As Figure 19 shows, the washers cover most of the diaphragm so that its motion closely approaches that of a true piston.

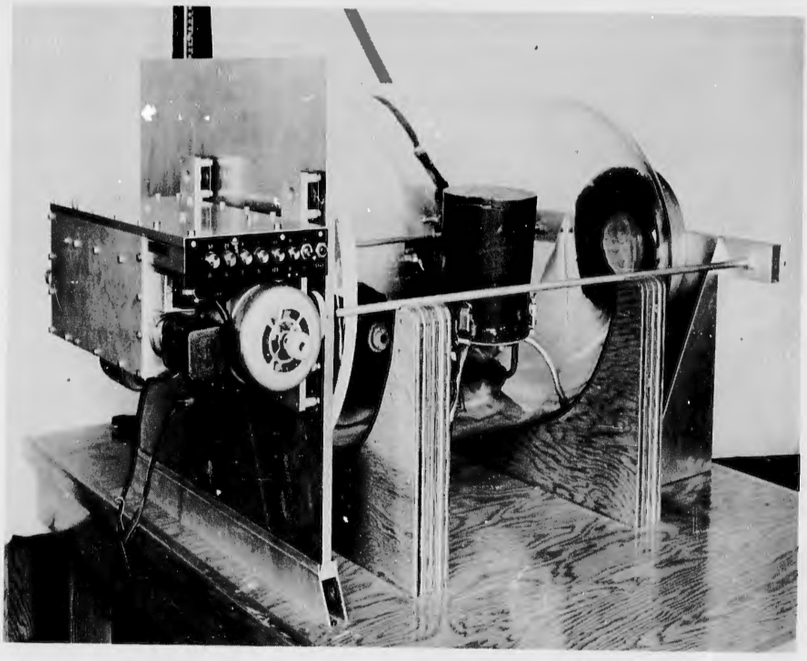

FIGURE 17. PISTONPHONE PUSHBUTTON FREQUENCY SELECTOR

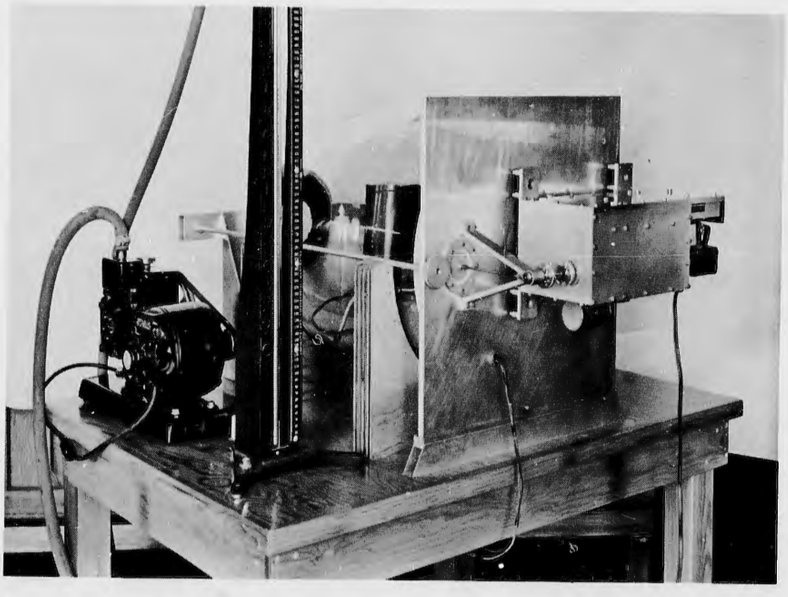

FIGURE 18. PISTONPHONE SEALED DIAPHRAGM AND GEARBOX

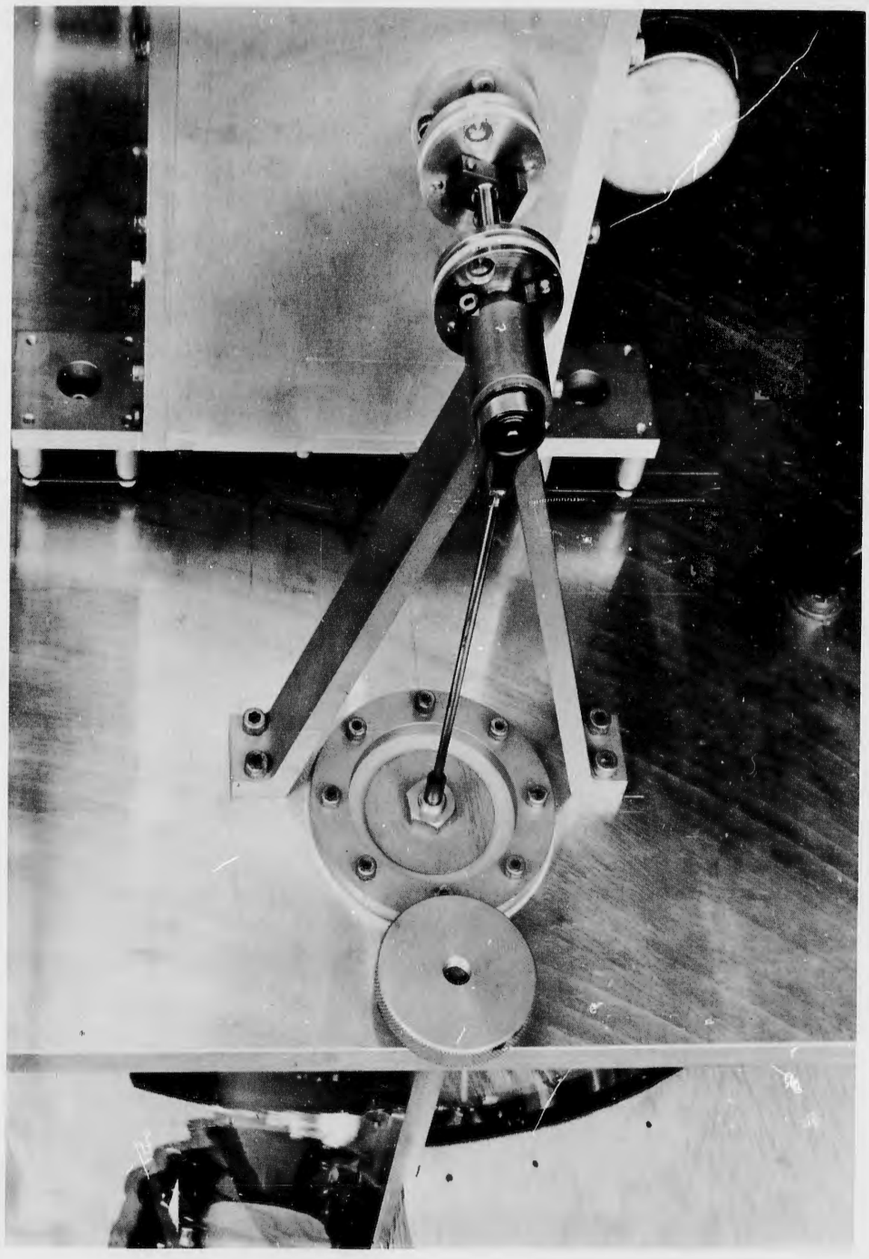

FIGURE 19. DETAIL OF SEALED DIAPHRAGM AND ECCENTRIC DRIVE

APPENDIX

The 25 spectrograms in this appendix show pressure spectrum levels vs. frequency for high-altitude acoustic background noise as sampled by free-floating, balloon-borne microphones during various days and seasons of the year. Below is a short description of the method by which these spectrograms were produced.

The preamplifier of each acoustic detector contained a 6 db/octave preemphasis network to compensate for the anticipated spectrum of background noise. Consequently, when the tape-recorded data was played back for analysis, it was first passed through a deemphasis network to restore the spectrum to its original shape. The tape to be analyzed was formed into a repeating loop of sufficient length to assure a good sampling of the lowest frequency present. Thus the playing time of each loop was at least three minutes. This loop was then played at very high speed in order to increase the recorded frequencies to the operating range of the spectrometer that was available.

The spectrometer used was a Bruel and Kjaer 1/3-octave analyzer covering a frequency range from 40 cps to 16 kc. Therefore the tape loops were played at 64 times the speed at which they were recorded. This, in effect, transformed the range of the analyzer to the 0.63- to 250-cps region. Finally, the 1/3-octave levels from the analyzer were converted to pressure-spectrum levels by using the expression

$$S = L - M - 10 \log \Delta f$$

where S = spectrum level in db relative to 1 dyne/cm^2 for a constant 1-cycle bandwidth, L = 1/3-octave level in db from the analyzer, M = output level of acoustic detector in db, Δf = 1/3 octave at frequency f, and 0 db = 1 volt/dyne/cm^2.

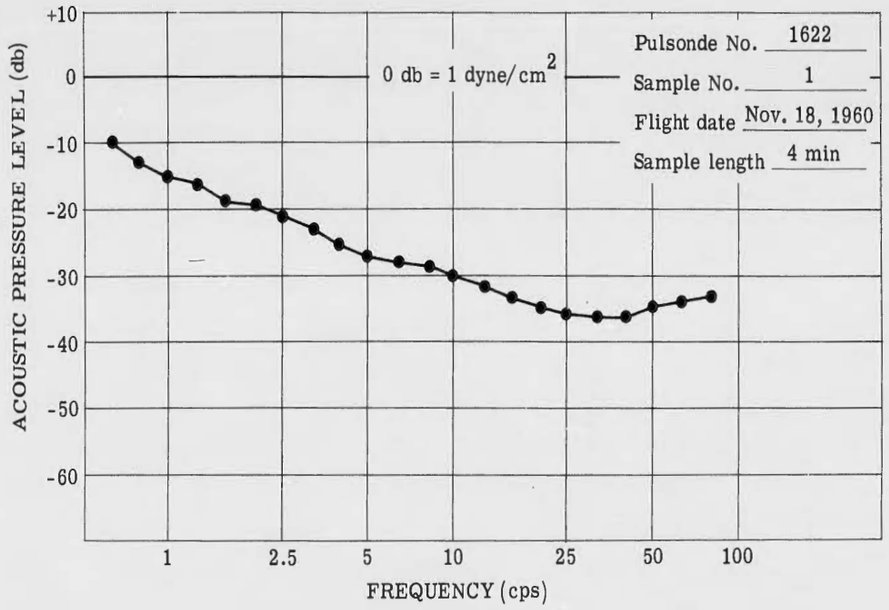

FIGURE A-1. ACOUSTIC PRESSURE SPECTRUM AT ALTITUDE OF 68,000 FEET

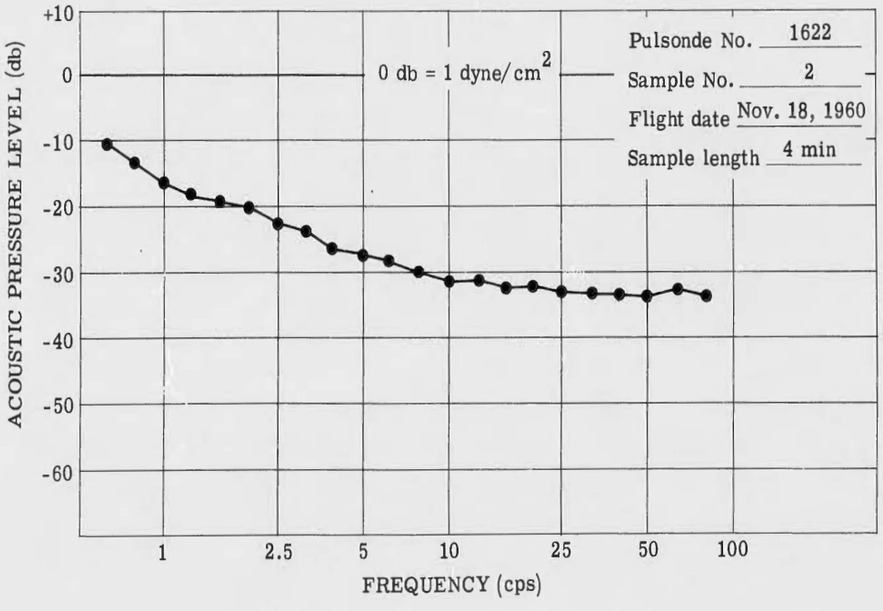

FIGURE A-2. ACOUSTIC PRESSURE SPECTRUM AT ALTITUDE OF 73,000 FEET

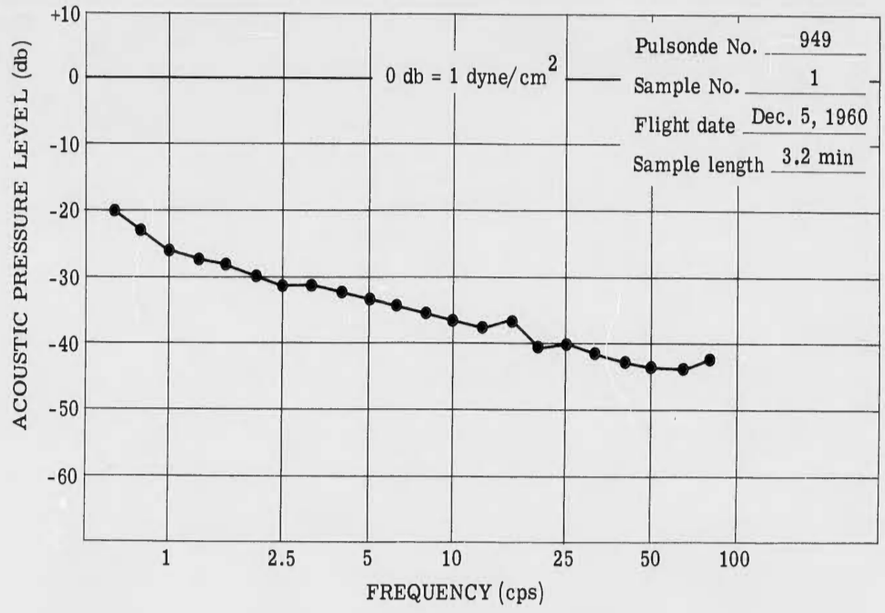

FIGURE A-3. ACOUSTIC PRESSURE SPECTRUM AT ALTITUDE OF 70,000 FEET

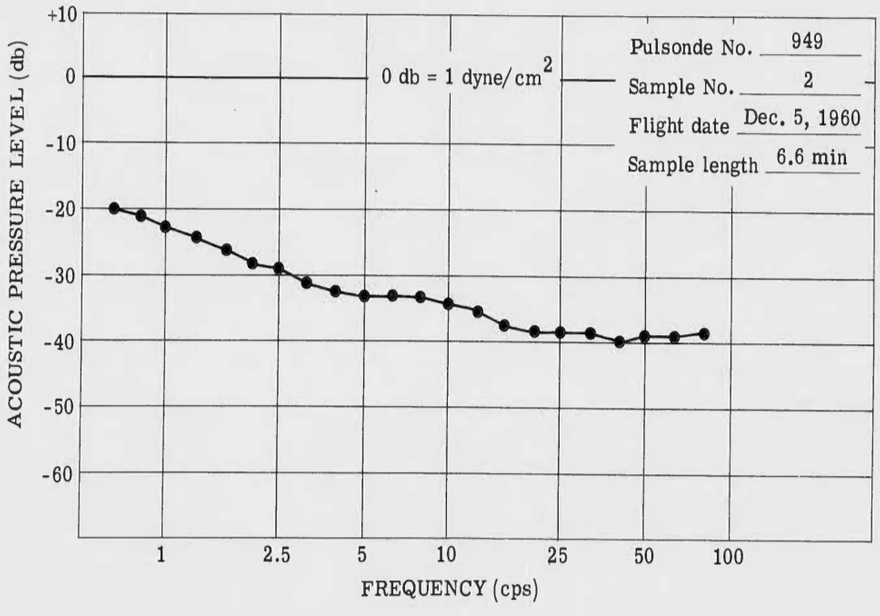

FIGURE A-4. ACOUSTIC PRESSURE SPECTRUM AT ALTITUDE OF 70,000 FEET

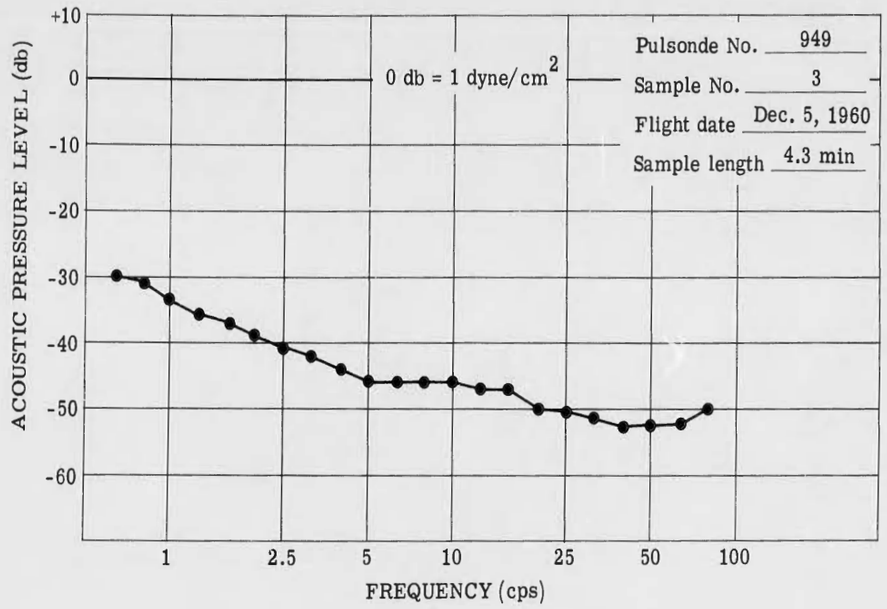

FIGURE A-5. ACOUSTIC PRESSURE SPECTRUM AT ALTITUDE OF 70,000 FEET

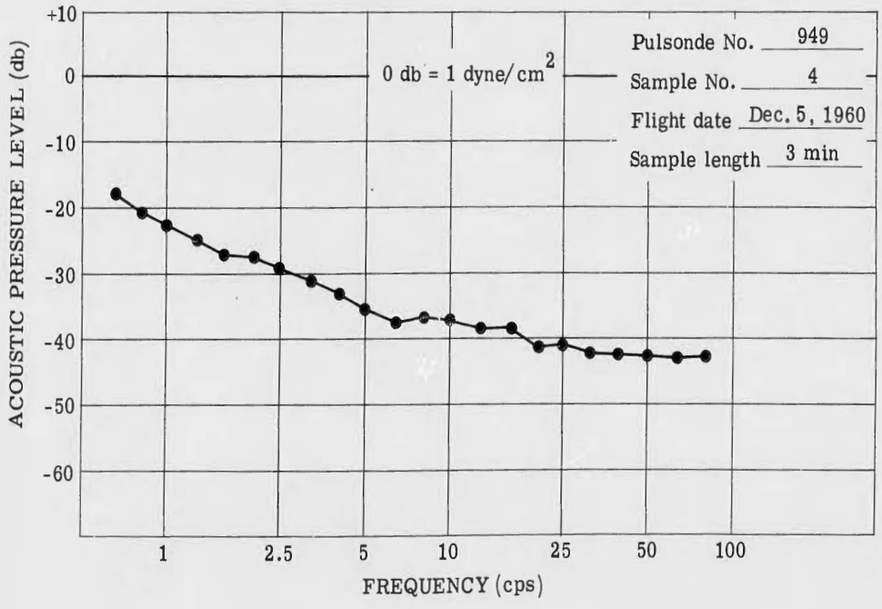

FIGURE A-6. ACOUSTIC PRESSURE SPECTRUM AT ALTITUDE OF 70,000 FEET

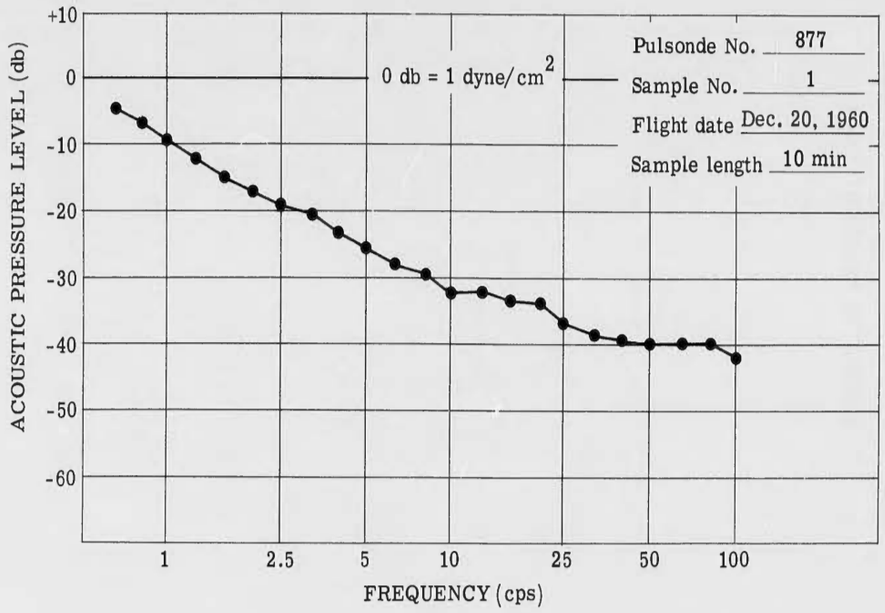

FIGURE A-7. ACOUSTIC PRESSURE SPECTRUM AT ALTITUDE OF 58,000 FEET

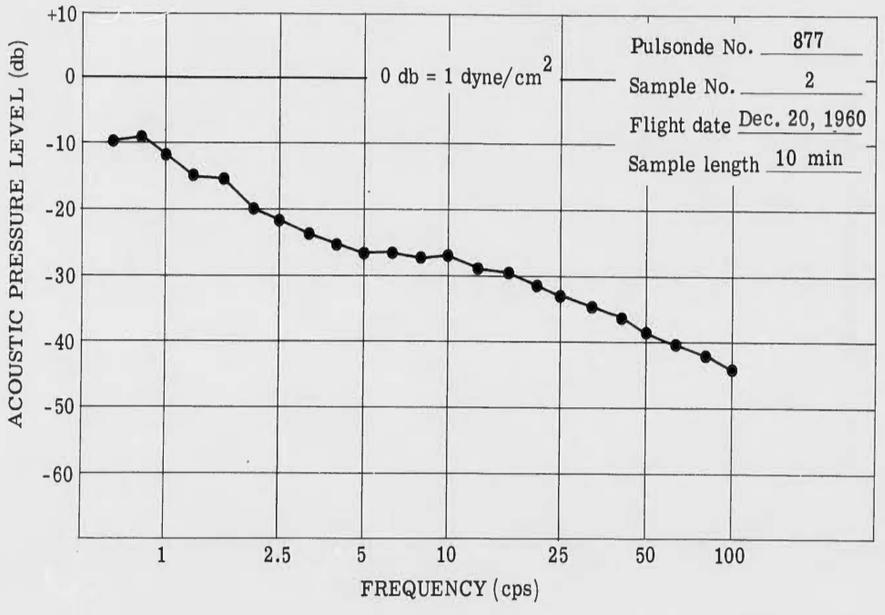

FIGURE A-8. ACOUSTIC PRESSURE SPECTRUM AT ALTITUDE OF 58,000 FEET

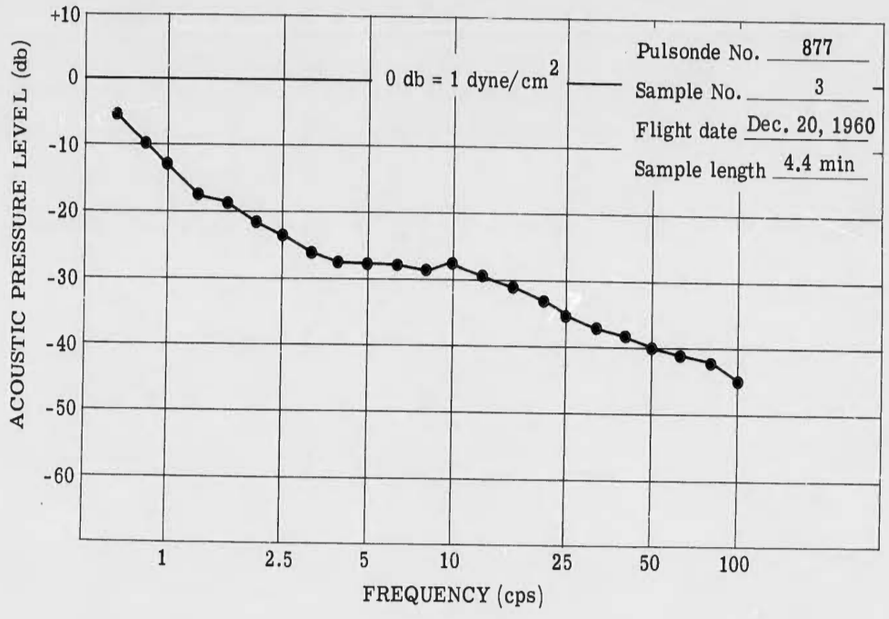

FIGURE A-9. ACOUSTIC PRESSURE SPECTRUM AT ALTITUDE OF 58,000 FEET

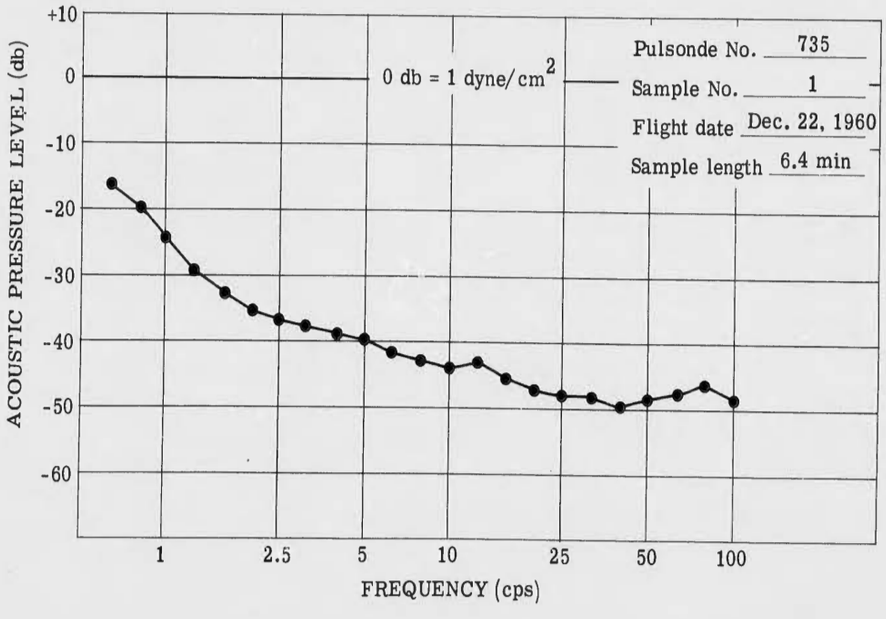

FIGURE A-10. ACOUSTIC PRESSURE SPECTRUM AT ALTITUDE OF 70,000 FEET

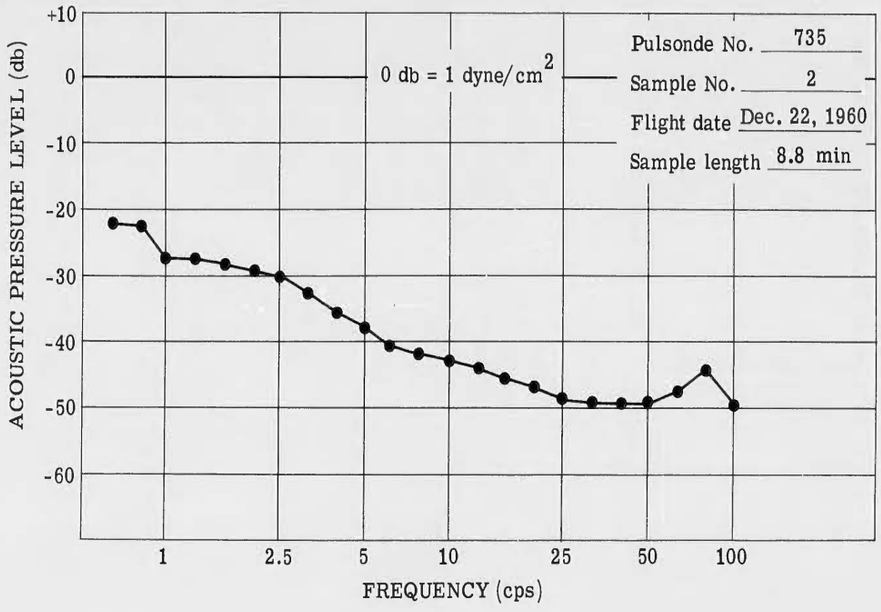

FIGURE A-11. ACOUSTIC PRESSURE SPECTRUM AT ALTITUDE OF 70,000 FEET

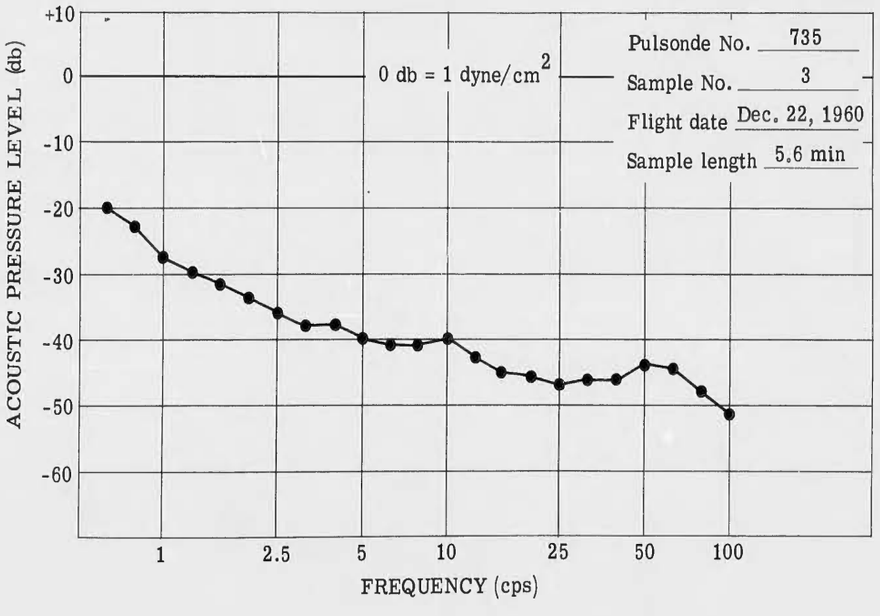

FIGURE A-12. ACOUSTIC PRESSURE SPECTRUM AT ALTITUDE OF 70,000 FEET

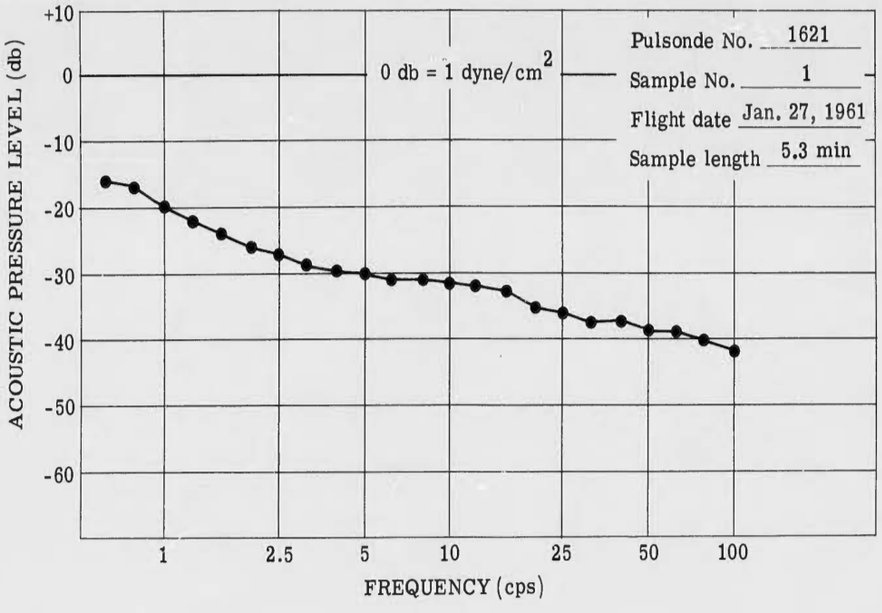

FIGURE A-13. ACOUSTIC PRESSURE SPECTRUM AT ALTITUDE OF 70,000 FEET

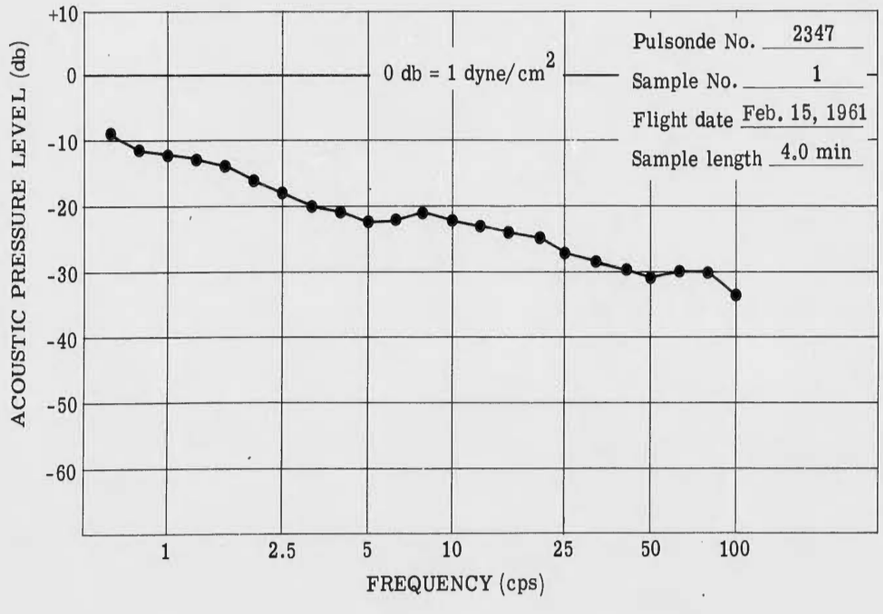

FIGURE A-14. ACOUSTIC PRESSURE SPECTRUM AT ALTITUDE OF 60,000 FEET

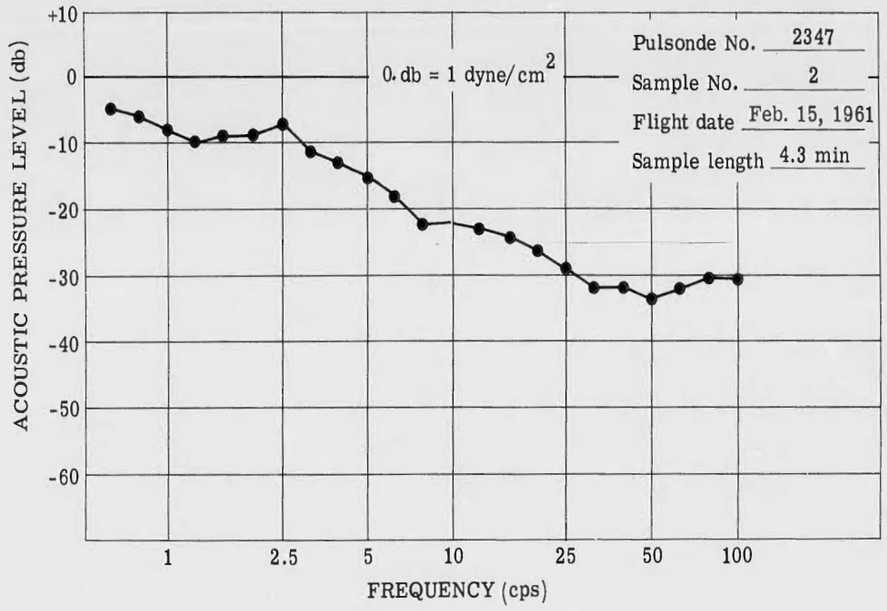

FIGURE A-15. ACOUSTIC PRESSURE SPECTRUM AT ALTITUDE OF 60,000 FEET

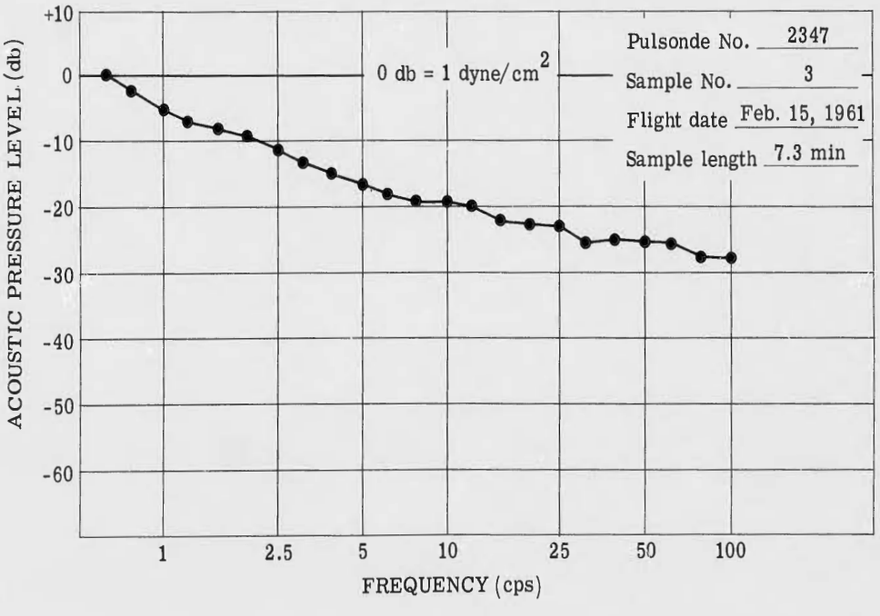

FIGURE A-16. ACOUSTIC PRESSURE SPECTRUM AT ALTITUDE OF 60,000 FEET

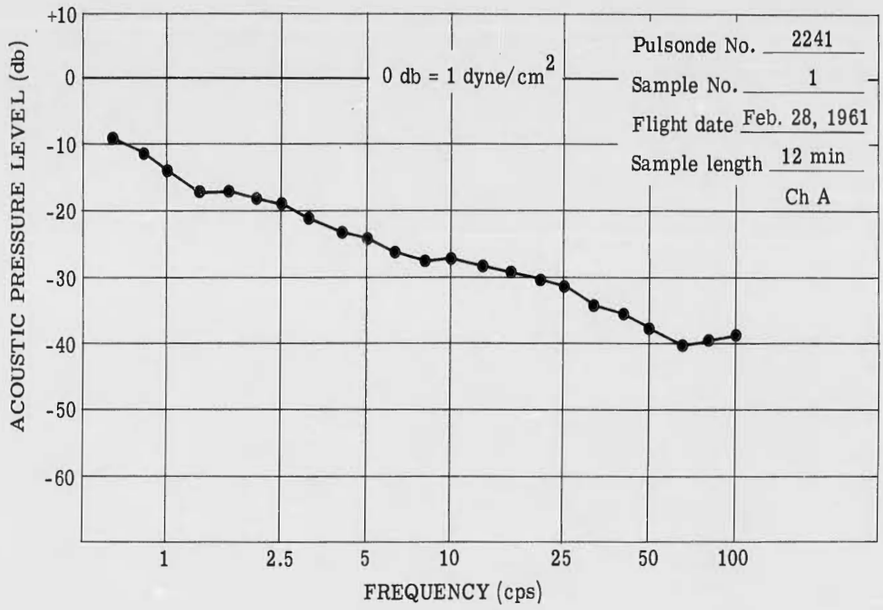

FIGURE A-17. ACOUSTIC PRESSURE SPECTRUM AT ALTITUDE OF 60,000 FEET

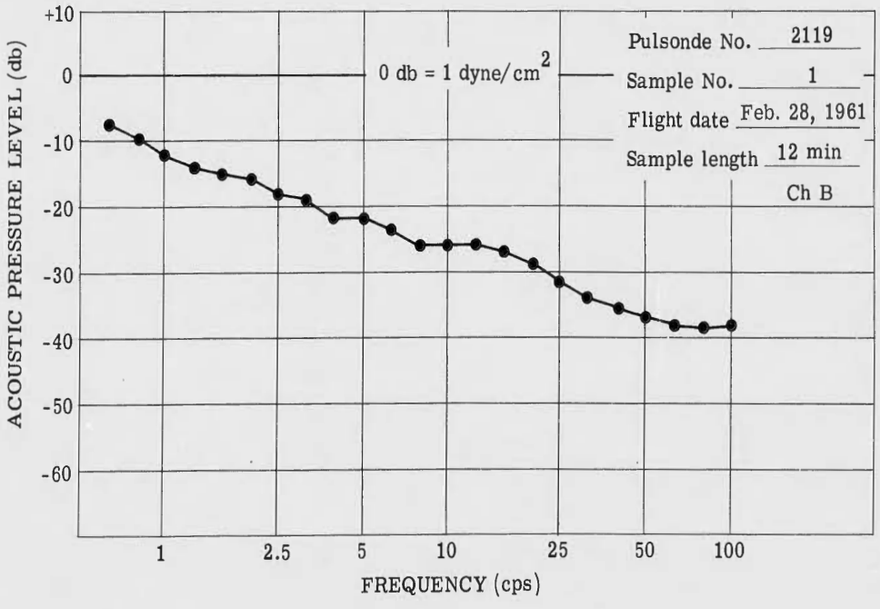

FIGURE A-18. ACOUSTIC PRESSURE SPECTRUM AT ALTITUDE OF 60,000 FEET

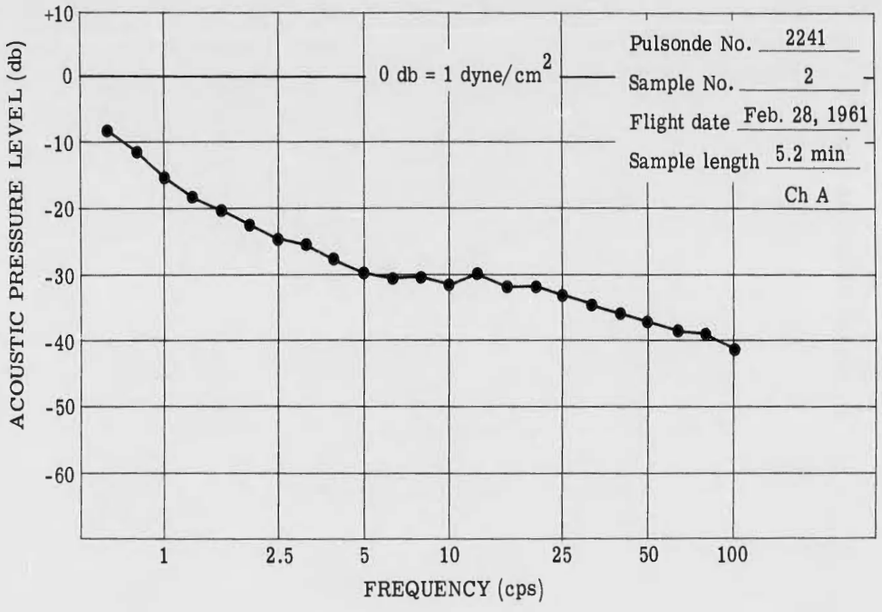

FIGURE A-19. ACOUSTIC PRESSURE SPECTRUM AT ALTITUDE OF 65,000 FEET

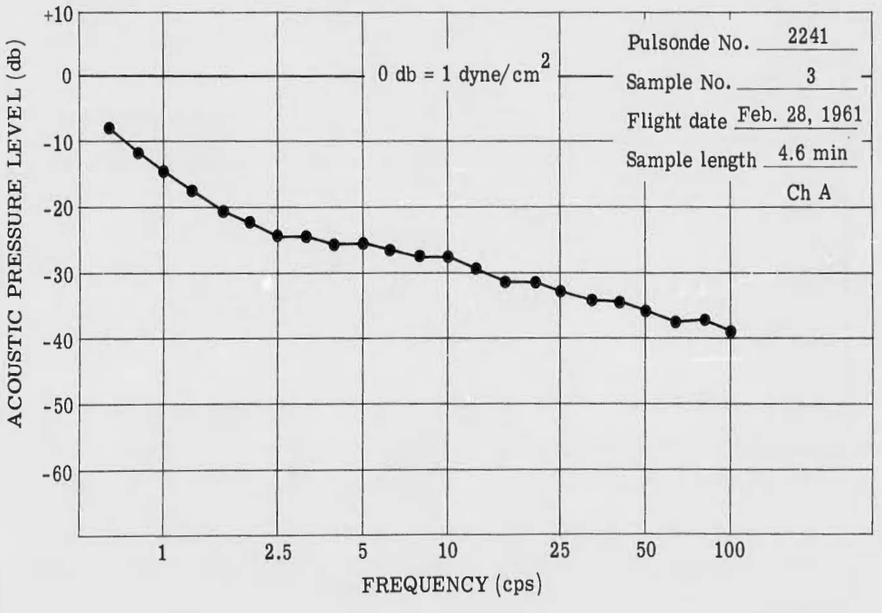

FIGURE A-20. ACOUSTIC PRESSURE SPECTRUM AT ALTITUDE OF 65,000 FEET

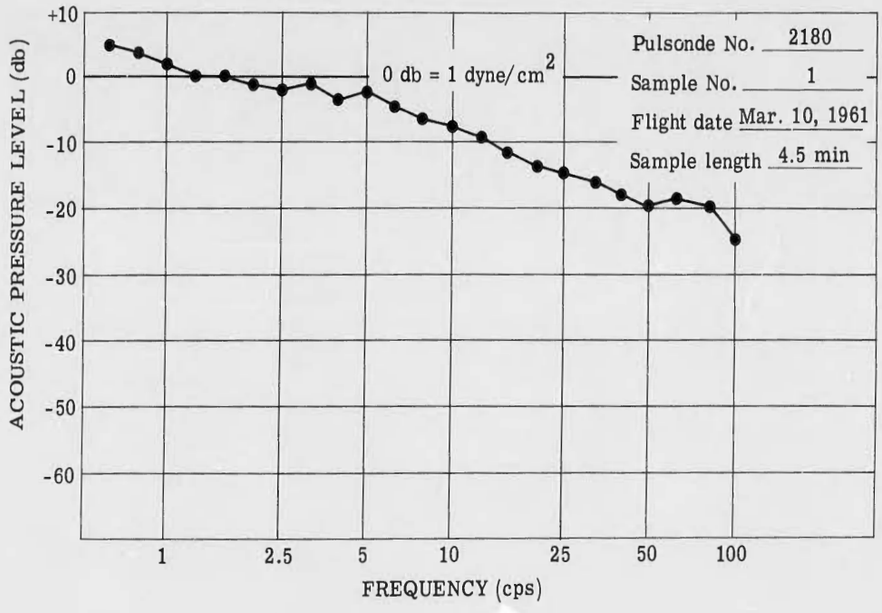

FIGURE A-21. ACOUSTIC PRESSURE SPECTRUM AT ALTITUDE OF 55,000 FEET

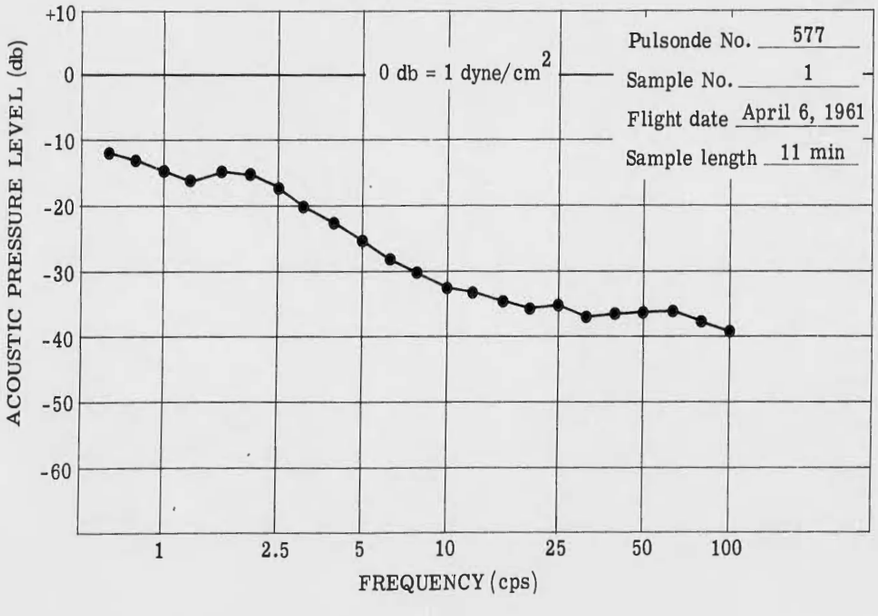

FIGURE A-22. ACOUSTIC PRESSURE SPECTRUM AT ALTITUDE OF 65,000 FEET

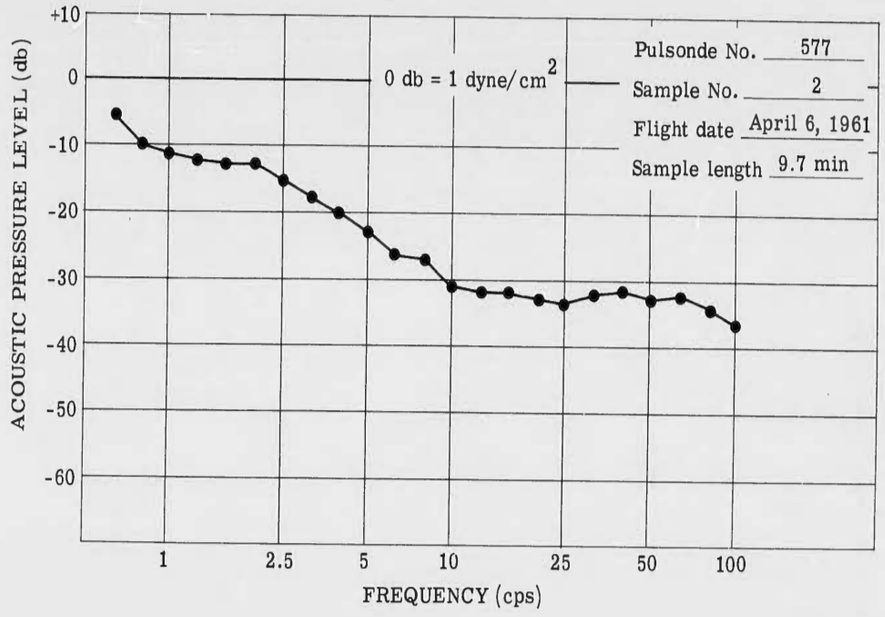

FIGURE A-23. ACOUSTIC PRESSURE SPECTRUM AT ALTITUDE OF 65,000 FEET

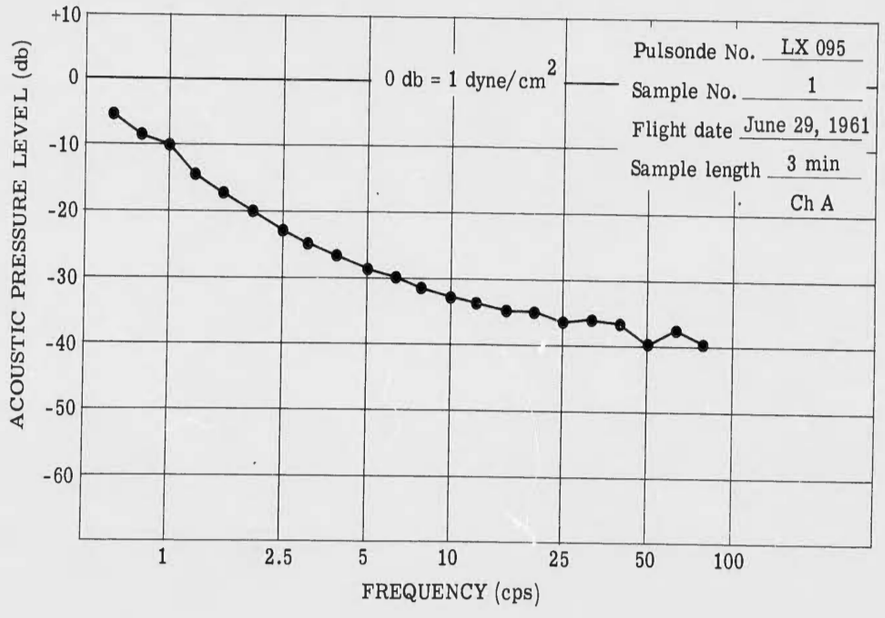

FIGURE A-24. ACOUSTIC PRESSURE SPECTRUM AT ALTITUDE OF 60,000 FEET

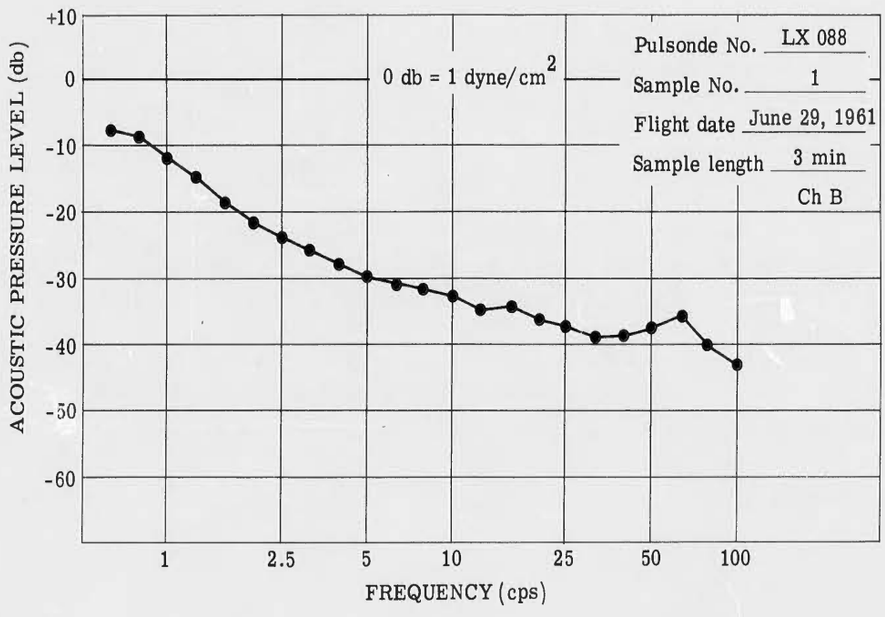

FIGURE A-25. ACOUSTIC PRESSURE SPECTRUM AT ALTITUDE OF 60,000 FEET

REFERENCES

1. J. W. Wescott, "Acoustic Background at High Altitudes," Proc. of Sympos. on Atmos. Acoustic Propagation, 1961, U. S. Army Sig. Missile Support Agency, White Sands, N. Mex., Vol. I, pp. 182-193, AD-408716.
2. W. C. Meecham, "Theory of Acoustic Background at High Altitudes," Proc. of Sympos. on Atmos. Acoustic Propagation, 1961, U. S. Army Sig. Missile Support Agency, White Sands, N. Mex., Vol. I, pp. 177-181, AD-408716.
3. W. C. Meecham and G. W. Ford, "Acoustic Radiation from Isotropic Turbulence," J. Acoust. Soc, Am., 1958, Vol. 30, pp. 318-322.
4. A. N. Kolmogoroff, "The Local Structure of Turbulence in Incompressible Viscous Fluid for Very Large Reynolds Numbers," C. R. Acad. Sci. URRS, 1941, Vol. 30, pp. 301-305.
5. P. B. MacCready, Jr., "Turbulence Measurements by Sailplane," J. Geophys. Research, 1962, Vol. 67, pp. 1041-1050.
6. P. B. MacCready, Jr., "The Inertial Subrange of Turbulence," J. Geophys. Research, 1962, Vol. 67, pp. 1051-1059.
7. J. W. Wescott and S. S. Kushner, Acoustic Background at the Earth's Surface, Rept. No. 3746-35-F, Inst. of Science and Technology, The University of Michigan, Ann Arbor, Mich., 1963, AD-405837.
8. P. B. MacCready, T. J. Lockhart, R. J. Diamond, and T. B. Smith, Atmospheric Turbulence Investigation by Sailplane, Tech. Rept. No. 56-279, Air Force Cambridge Research Center, Bedford, Mass., 1956, AD-98701.
9. H. Press, Atmospheric Turbulence Environment with Special Reference to Continuous Turbulence, Rept. No. 115, NATO, Advisory Group for Aeronautical Res. & Dev., 1957.
10. K. D. Saunders, B-66B Low Level Gust Study, I, Technical Analysis, Tech. Rept. No. 60-305, Wright Air Dev. Div., Dayton, Ohio, 1961.
11. G. K. Batchelor, "The Application of the Similarity Theory of Turbulence to Atmospheric Diffusion," Quart. J. Meteorol. Soc., 1950, Vol. 76, pp. 133-146.
12. F. B. Daniels, "Acoustical Energy Generated by the Ocean Waves," J. Acoust. Soc. Am., 1952, Vol. 24, p. 83.
13. R. K. Cook and J. M. Young, "Strange Sounds in the Atmosphere, Part II," Sound, 1962, Vol. 1, No. 3, pp. 25-33.
14. H. Benioff and B. Gutenberg, "Observations with Electromagnetic Microbarographs," Nature, 1939, Vol. 144, p. 478.
15. W. L. Webb, J. W. Coffman, and G. Q. Clark, A High-Altitude Acoustic Sensing System, Special Rept. No. 28, U. S. Army Signal Missile Support Agency, White Sands, N. Mex., 38 pp., 1959, AD-230726L.
16. C. McDonald and G. Q. Clark, Modification of Radiosonde AN/AMT-4A to Monitor Acoustic Data, Schellenger Research Laboratory, Texas Western College, El Paso, 30 pp., 1960.

17. F. L. Fugate, Pulsonde Acoustical Sensing Device, Schellenger Research Laboratory, Texas Western College, El Paso, 96 pp., 1960.

18. Dept. of the Army, Radiosonde AN/AMT-4A, Tech. Manual No. TM 11-2432A, U. S. Gov't. Printing Office, Washington, D. C., 51 pp., 1958.

19. Dept. of the Army, Rawin Set AN/GMD-1A, Tech. Manual No. TM 11-271A, U. S. Gov't. Printing Office, Washington, D. C., 367 pp., 1954.

DISTRIBUTION LIST

Copy No.	Addressee
1-100	Contracting Officer White Sands Missile Range, New Mexico ATTN: ORDBS-P&C-C-N
101-110	Mr. Marvin Diamond U. S. Army Electronics R&D Activity White Sands Missile Range, New Mexico ATTN: SELWS-M
111-112	Contracting Officer Detroit Ordnance District 1580 East Grand Blvd. Detroit 11, Michigan
113-117	Prof. Thomas G. Barnes, Director Schellenger Research Laboratory Texas Western College El Paso, Texas
118-127	Defense Documentation Center Cameron Station Alexandria, Virginia 22314

AD Div. 25/1

Inst. of Science and Technology, U. of Mich., Ann Arbor
ACOUSTIC DETECTION OF HIGH-ALTITUDE TURBULENCE by John W. Wescott. Mar. 64. 49 p. incl. illus., 19 refs.
(Report No. 3746-38-T)
(Contract DA-20-018-ORD-22840) Unclassified report

Background noise at frequencies from 0.2 to 200 cps was monitored with free-floating, balloon-borne acoustic probes at altitudes of 55,000 to 73,000 feet. Spectrograms, signatures, cross-correlations, and probability-density curves were obtained from the data. The noise has a spectrum with 6 db/octave negative slope, is acoustic and Gaussian, and is time-steady for periods of several hours, although noise pressures from 0.03 to 1 dyne/cm^2 were measured on different days. These

(over)

UNCLASSIFIED

I. Wescott, John W.
II. U. S. Army Electronics Research and Development Activity
III. Contract DA-20-018-ORD-22840

Defense Documentation Center
UNCLASSIFIED

AD Div. 25/1

Inst. of Science and Technology, U. of Mich., Ann Arbor
ACOUSTIC DETECTION OF HIGH-ALTITUDE TURBULENCE by John W. Wescott. Mar. 64. 49 p. incl. illus., 19 refs.
(Report No. 3746-38-T)
(Contract DA-20-018-ORD-22840) Unclassified report

Background noise at frequencies from 0.2 to 200 cps was monitored with free-floating, balloon-borne acoustic probes at altitudes of 55,000 to 73,000 feet. Spectrograms, signatures, cross-correlations, and probability-density curves were obtained from the data. The noise has a spectrum with 6 db/octave negative slope, is acoustic and Gaussian, and is time-steady for periods of several hours, although noise pressures from 0.03 to 1 dyne/cm^2 were measured on different days. These

(over)

UNCLASSIFIED

I. Wescott, John W.
II. U. S. Army Electronics Research and Development Activity
III. Contract DA-20-018-ORD-22840

Defense Documentation Center
UNCLASSIFIED

AD Div. 25/1

Inst. of Science and Technology, U. of Mich., Ann Arbor
ACOUSTIC DETECTION OF HIGH-ALTITUDE TURBULENCE by John W. Wescott. Mar. 64. 49 p. incl. illus., 19 refs.
(Report No. 3746-38-T)
(Contract DA-20-018-ORD-22840) Unclassified report

Background noise at frequencies from 0.2 to 200 cps was monitored with free-floating, balloon-borne acoustic probes at altitudes of 55,000 to 73,000 feet. Spectrograms, signatures, cross-correlations, and probability-density curves were obtained from the data. The noise has a spectrum with 6 db/octave negative slope, is acoustic and Gaussian, and is time-steady for periods of several hours, although noise pressures from 0.03 to 1 dyne/cm^2 were measured on different days. These

(over)

UNCLASSIFIED

I. Wescott, John W.
II. U. S. Army Electronics Research and Development Activity
III. Contract DA-20-018-ORD-22840

Defense Documentation Center
UNCLASSIFIED

AD Div. 25/1

Inst. of Science and Technology, U. of Mich., Ann Arbor
ACOUSTIC DETECTION OF HIGH-ALTITUDE TURBULENCE by John W. Wescott. Mar. 64. 49 p. incl. illus., 19 refs.
(Report No. 3746-38-T)
(Contract DA-20-018-ORD-22840) Unclassified report

Background noise at frequencies from 0.2 to 200 cps was monitored with free-floating, balloon-borne acoustic probes at altitudes of 55,000 to 73,000 feet. Spectrograms, signatures, cross-correlations, and probability-density curves were obtained from the data. The noise has a spectrum with 6 db/octave negative slope, is acoustic and Gaussian, and is time-steady for periods of several hours, although noise pressures from 0.03 to 1 dyne/cm^2 were measured on different days. These

(over)

UNCLASSIFIED

I. Wescott, John W.
II. U. S. Army Electronics Research and Development Activity
III. Contract DA-20-018-ORD-22840

Defense Documentation Center
UNCLASSIFIED

AD

and other results indicate that the noise comes from lower altitudes and is produced by an array of statistically independent radiators, such as turbulent eddies.

A theory for the power spectrum of noise radiated by turbulence is cited, and the predicted spectrum is compared to the experimental results. Other possible sources of the high-altitude acoustic noise are described. Descriptions and illustrations of the instruments used to acquire and process the experimental data are presented.

UNCLASSIFIED

DESCRIPTORS

Acoustics
Acoustic equipment
Atmospheric motion
Balloons
Detection
Lightning
Magnetic storms
Microphones
Noise
Ocean waves
Probability
Seismic waves
Tornadoes
Turbulence
Tracking
Tropical cyclones

UNCLASSIFIED

AD

and other results indicate that the noise comes from lower altitudes and is produced by an array of statistically independent radiators, such as turbulent eddies.

A theory for the power spectrum of noise radiated by turbulence is cited, and the predicted spectrum is compared to the experimental results. Other possible sources of the high-altitude acoustic noise are described. Descriptions and illustrations of the instruments used to acquire and process the experimental data are presented.

UNCLASSIFIED

DESCRIPTORS

Acoustics
Acoustic equipment
Atmospheric motion
Balloons
Detection
Lightning
Magnetic storms
Microphones
Noise
Ocean waves
Probability
Seismic waves
Tornadoes
Turbulence
Tracking
Tropical cyclones

UNCLASSIFIED

AD

and other results indicate that the noise comes from lower altitudes and is produced by an array of statistically independent radiators, such as turbulent eddies.

A theory for the power spectrum of noise radiated by turbulence is cited, and the predicted spectrum is compared to the experimental results. Other possible sources of the high-altitude acoustic noise are described. Descriptions and illustrations of the instruments used to acquire and process the experimental data are presented.

UNCLASSIFIED

DESCRIPTORS

Acoustics
Acoustic equipment
Atmospheric motion
Balloons
Detection
Lightning
Magnetic storms
Microphones
Noise
Ocean waves
Probability
Seismic waves
Tornadoes
Turbulence
Tracking
Tropical cyclones

UNCLASSIFIED

AD

and other results indicate that the noise comes from lower altitudes and is produced by an array of statistically independent radiators, such as turbulent eddies.

A theory for the power spectrum of noise radiated by turbulence is cited, and the predicted spectrum is compared to the experimental results. Other possible sources of the high-altitude acoustic noise are described. Descriptions and illustrations of the instruments used to acquire and process the experimental data are presented.

UNCLASSIFIED

DESCRIPTORS

Acoustics
Acoustic equipment
Atmospheric motion
Balloons
Detection
Lightning
Magnetic storms
Microphones
Noise
Ocean waves
Probability
Seismic waves
Tornadoes
Turbulence
Tracking
Tropical cyclones

UNCLASSIFIED

AD Div. 25/1

Inst. of Science and Technology, U. of Mich., Ann Arbor
ACOUSTIC DETECTION OF HIGH-ALTITUDE TURBULENCE by John W. Wescott. Mar. 64. 49 p. incl. illus., 19 refs.
(Report No. 3746-38-T)
(Contract DA-20-018-ORD-22840) Unclassified report

Background noise at frequencies from 0.2 to 200 cps was monitored with free-floating, balloon-borne acoustic probes at altitudes of 55,000 to 73,000 feet. Spectrograms, signatures, cross-correlations, and probability-density curves were obtained from the data. The noise has a spectrum with 6 db/octave negative slope, is acoustic and Gaussian, and is time-steady for periods of several hours, although noise pressures from 0.03 to 1 dyne/cm^2 were measured on different days. These

(over)

UNCLASSIFIED

I. Wescott, John W.
II. U. S. Army Electronics Research and Development Activity
III. Contract DA-20-018-ORD-22840

Defense Documentation Center
UNCLASSIFIED

AD Div. 25/1

Inst. of Science and Technology, U. of Mich., Ann Arbor
ACOUSTIC DETECTION OF HIGH-ALTITUDE TURBULENCE by John W. Wescott. Mar. 64. 49 p. incl. illus., 19 refs.
(Report No. 3746-38-T)
(Contract DA-20-018-ORD-22840) Unclassified report

Background noise at frequencies from 0.2 to 200 cps was monitored with free-floating, balloon-borne acoustic probes at altitudes of 55,000 to 73,000 feet. Spectrograms, signatures, cross-correlations, and probability-density curves were obtained from the data. The noise has a spectrum with 6 db/octave negative slope, is acoustic and Gaussian, and is time-steady for periods of several hours, although noise pressures from 0.03 to 1 dyne/cm^2 were measured on different days. These

(over)

UNCLASSIFIED

I. Wescott, John W.
II. U. S. Army Electronics Research and Development Activity
III. Contract DA-20-018-ORD-22840

Defense Documentation Center
UNCLASSIFIED

AD Div. 25/1

Inst. of Science and Technology, U. of Mich., Ann Arbor
ACOUSTIC DETECTION OF HIGH-ALTITUDE TURBULENCE by John W. Wescott. Mar. 64. 49 p. incl. illus., 19 refs.
(Report No. 3746-38-T)
(Contract DA-20-018-ORD-22840) Unclassified report

Background noise at frequencies from 0.2 to 200 cps was monitored with free-floating, balloon-borne acoustic probes at altitudes of 55,000 to 73,000 feet. Spectrograms, signatures, cross-correlations, and probability-density curves were obtained from the data. The noise has a spectrum with 6 db/octave negative slope, is acoustic and Gaussian, and is time-steady for periods of several hours, although noise pressures from 0.03 to 1 dyne/cm^2 were measured on different days. These

(over)

UNCLASSIFIED

I. Wescott, John W.
II. U. S. Army Electronics Research and Development Activity
III. Contract DA-20-018-ORD-22840

Defense Documentation Center
UNCLASSIFIED

AD Div. 25/1

Inst. of Science and Technology, U. of Mich., Ann Arbor
ACOUSTIC DETECTION OF HIGH-ALTITUDE TURBULENCE by John W. Wescott. Mar. 64. 49 p. incl. illus., 19 refs.
(Report No. 3746-38-T)
(Contract DA-20-018-ORD-22840) Unclassified report

Background noise at frequencies from 0.2 to 200 cps was monitored with free-floating, balloon-borne acoustic probes at altitudes of 55,000 to 73,000 feet. Spectrograms, signatures, cross-correlations, and probability-density curves were obtained from the data. The noise has a spectrum with 6 db/octave negative slope, is acoustic and Gaussian, and is time-steady for periods of several hours, although noise pressures from 0.03 to 1 dyne/cm^2 were measured on different days. These

(over)

UNCLASSIFIED

I. Wescott, John W.
II. U. S. Army Electronics Research and Development Activity
III. Contract DA-20-018-ORD-22840

Defense Documentation Center
UNCLASSIFIED

AD

and other results indicate that the noise comes from lower altitudes and is produced by an array of statistically independent radiators, such as turbulent eddies.

A theory for the power spectrum of noise radiated by turbulence is cited, and the predicted spectrum is compared to the experimental results. Other possible sources of the high-altitude acoustic noise are described. Descriptions and illustrations of the instruments used to acquire and process the experimental data are presented.

UNCLASSIFIED

DESCRIPTORS

Acoustics
Acoustic equipment
Atmospheric motion
Balloons
Detection
Lightning
Magnetic storms
Microphones
Noise
Ocean waves
Probability
Seismic waves
Tornadoes
Turbulence
Tracking
Tropical cyclones

UNCLASSIFIED

AD

and other results indicate that the noise comes from lower altitudes and is produced by an array of statistically independent radiators, such as turbulent eddies.

A theory for the power spectrum of noise radiated by turbulence is cited, and the predicted spectrum is compared to the experimental results. Other possible sources of the high-altitude acoustic noise are described. Descriptions and illustrations of the instruments used to acquire and process the experimental data are presented.

UNCLASSIFIED

DESCRIPTORS

Acoustics
Acoustic equipment
Atmospheric motion
Balloons
Detection
Lightning
Magnetic storms
Microphones
Noise
Ocean waves
Probability
Seismic waves
Tornadoes
Turbulence
Tracking
Tropical cyclones

UNCLASSIFIED

+

AD

and other results indicate that the noise comes from lower altitudes and is produced by an array of statistically independent radiators, such as turbulent eddies.

A theory for the power spectrum of noise radiated by turbulence is cited, and the predicted spectrum is compared to the experimental results. Other possible sources of the high-altitude acoustic noise are described. Descriptions and illustrations of the instruments used to acquire and process the experimental data are presented.

UNCLASSIFIED

DESCRIPTORS

Acoustics
Acoustic equipment
Atmospheric motion
Balloons
Detection
Lightning
Magnetic storms
Microphones
Noise
Ocean waves
Probability
Seismic waves
Tornadoes
Turbulence
Tracking
Tropical cyclones

UNCLASSIFIED

AD

and other results indicate that the noise comes from lower altitudes and is produced by an array of statistically independent radiators, such as turbulent eddies.

A theory for the power spectrum of noise radiated by turbulence is cited, and the predicted spectrum is compared to the experimental results. Other possible sources of the high-altitude acoustic noise are described. Descriptions and illustrations of the instruments used to acquire and process the experimental data are presented.

UNCLASSIFIED

DESCRIPTORS

Acoustics
Acoustic equipment
Atmospheric motion
Balloons
Detection
Lightning
Magnetic storms
Microphones
Noise
Ocean waves
Probability
Seismic waves
Tornadoes
Turbulence
Tracking
Tropical cyclones

UNCLASSIFIED

UNCLASSIFIED